Ca^{2+}-dependent inactivation of a neuronal Ca^{2+} channel is regulated by intracellular Ca^{2+} handling

by

Eammon Keith MacNeil

A thesis submitted to the Graduate Program in

Biomedical and Molecular Sciences

in conformity with the requirements for

the degree of Master of Science

Queen's University

Kingston, Ontario, Canada

December 2023

Abstract

Intracellular Ca^{2+} is a critical regulator of gene expression, neuronal excitability, and neurosecretion. Free cytosolic Ca^{2+} is controlled by numerous channels, pumps, and exchangers in the plasma membrane, endoplasmic reticulum, or mitochondria. In the marine mollusc, *Aplysia californica*, ovulation is initiated from the central nervous system by bag cell neurons. Upon brief synaptic input, these neuroendocrine cells fire a synchronous afterdischarge, starting with an ~5-Hz, ~1-min fast-phase, then an ~1-Hz, ~30-min slow-phase, that culminates in the Ca^{2+}-dependent neurohaemal secretion of egg-laying hormone. During the fast-phase, Ca^{2+} rises due to entry through voltage-gated Ca^{2+} channels. Repetitive opening results in Ca^{2+}-dependent inactivation (CDI) of the channel, aka use-dependent rundown, which serves as a form of negative feedback. Our laboratory previously showed that mitochondria sequester voltage-gated Ca^{2+} influx, although how this influences Ca^{2+} channel function is unknown. Here, I test the hypothesis that intracellular Ca^{2+} handling, by both membrane transport and organelles, controls CDI. Rundown of isolated Ca^{2+} current was recorded in single cultured bag cell neurons under whole-cell voltage-clamp using recurring step depolarizations (~70% current remaining at the end of a 5-Hz, 5-sec train-stimulus). Rundown was significantly decreased by swapping Ba^{2+} for Ca^{2+} in the external solution, or adding the Ca^{2+} chelator, EGTA, to the intracellular/pipette solution (both ~90% current remaining). However, blocking either the mitochondrial Ca^{2+} uniporter or the plasma membrane Ca^{2+}-ATPase significantly increased rundown (both ~60% current remaining). To further understand mitochondrial Ca^{2+} handling, neurons were loaded with the Ca^{2+} sensitive dye, fura-PE3, and Ca^{2+} liberated from the mitochondria by collapsing the organelle membrane potential with the protonophore, carbonyl cyanide 4-(trifluoromethoxy) phenylhydrazone (FCCP). Compared to control, a prior train-stimulus to elicit

Ca^{2+} entry significantly increased the FCCP-induced percent-change in Ca^{2+} (from ~175% to ~450%), and this was prevented by inhibiting the mitochondrial Ca^{2+} uniporter. These findings suggest that both mitochondrial uptake and plasma membrane extrusion play a key role in CDI by buffering Ca^{2+} during prolonged influx. Overall, Ca^{2+} dynamics serve as a key regulator of Ca^{2+} channel function, with the potential to govern Ca^{2+}-dependent processes in general.

Co-Authorship

The following thesis expands on preliminary discoveries made in our laboratory by Dr. Neil Magoski and Dr. Chris Groten. Dr. Magoski provided me with training in whole-cell voltage-clamp recording and fluorescent microscopy. Dr. Magoski and I discussed on a regular basis my results and observations, experimental procedures, and relevant literature. Experimental design was a combined effort between Dr. Magoski and myself.

I performed all data recording and analyses. Figures 5 and 6 are modified from Dr. Groten's thesis. I prepared most of my own solutions and drugs, however, my fellow lab members also provided assistance in common solution preparation. In addition, Dr. Magoksi, Dr. Alamjeet Kaur Chauhan-Puri, Jennifer Li, Kelly Lee, and Alex Prosserman provided animal care services. Most bag cell neuron cultures used were prepared by myself; however, some neurons were prepared by fellow lab members. Animal dissections and removal of the abdominal ganglia were shared between myself and other members of the lab.

I prepared this thesis and all of its contents with necessary editing, proofreading, and constructive criticism from Dr. Magoski.

Acknowledgements

First and foremost, I would like to express my heartfelt gratitude to Dr. Magoski, who provided boundless support throughout my undergraduate and graduate research experience. Thank you for sharing your wealth of knowledge and enthusiasm for science – your passion and dedication to research, and those under your tutelage, is palpable and is something I can only hope to pay forward in-kind.

I am grateful to my fellow members of the Magoski Lab, Alamjeet Kaur Chauhan-Puri, Jennifer Li, Kelly Lee, and Alex Prosserman. Thank you for making the lab a welcoming and fun place to work; It was a pleasure to learn from, and with you all.

Finally, I'd like to thank my family and friends for their love and support throughout my education. To my late mother, Christine, thank you for giving me your passion for learning and teaching me to always strive for more. These have been and will continue to be guiding principles in my life. To my father, Bern, thank you for instilling in me the virtues of hard work and dedication. Without these, and your guidance, I would not have achieved what I have today.

Table of Contents

List of Figures

List of Abbreviations

ºC	degree Celsius
µg	microgram
µl	microlitre
µm	micrometer
µM	micromolar
A	alanine
Apl	*Aplysia*
ASW	artificial seawater
ATP	adenosine triphosphate
Ba^{2+}	barium ion
$BaCl_2$	barium chloride
Ca^{2+}	calcium ion
$CaCl_2$	calcium chloride
CaM	calmodulin
CDI	calcium dependent inactivation
CE	carboxyeosin
CICR	calcium-induced calcium release
Cl^-	chloride ion
Co^{2+}	cobalt ion
CRE	calcium response element
CREB	CRE binding protein
Cs^+	caesium ion
CsCl	caesium chloride
CsOH	caesium hydroxide
d	day
DMSO	dimethyl sulfoxide
DRG	dorsal root ganglion
eEPSP	early excitatory postsynaptic potential
EGTA	ethyleneglycol bis (aminoethylether) tetraacetic acid
ELH	egg-laying hormone
F	phenylalanine
FCCP	carbonyl cyanide 4-(trifluoromethoxy) phenylhydrazone
Fig	figure
g	gram
GTP	guanosine triphosphate
HEPES	15 4-(2-hydroxyethyl)-1-piperazineethanesulfonic acid
hr	hour
Hz	hertz

I/V	current voltage relationship
K^+	potassium
KCl	potassium chloride
kD	kilodalton
kHz	kilohertz
L	litre
La^{3+}	lanthanum ion
MCU	mitochondrial calcium uniporter
mEPSP	miniature excitatory postsynaptic potential
mg	milligram
$MgCl_2$	magnesium chloride
min	minute
ml	milliliter
mM	millimolar
mm	millimeter
ms	millisecond
mV	millivolt
MW	molecular weight
MΩ	megaohm
n	sample number
Na^+	sodium ion
NaCl	sodium chloride
NaOH	sodium hydroxide
ng	nanogram
Ni^{2+}	nickel ion
nM	nanomolar
pF	picofarad
pKa	dissociation constant
PKC	protein kinase C
PMCA	plasma membrane calcium-ATPase
ROI	region of interest
Ru360	ruthenium 360
S	serine
sec	second
SERCA	endoplasmic reticulum calcium-ATPase
SNAP-25	synaptosome-associated-protein of 25-kDa
tcASW	tissue culture artificial sea water
TEA	tetraethylammonium
TPP	tetraphenylphosphonium chloride
TRP	transient receptor potential

$V_{1/2}$	mid-activation voltage
VDI	voltage-dependent inactivation
wk	week
Xe	xenon
Y	tyrosine
Zn^{+}	zinc ion

Chapter 1 - Introduction

Ca^{2+} Signaling

Intracellular Ca^{2+} is a critical biochemical signal responsible for the regulation of many key physiological processes, such as neuronal excitability, gene expression, and secretion (Clapham 2007; Giorgi et al. 2018). Particularly in the nervous system, Ca^{2+} signaling is not only essential in the operation of cellular machinery, but the differentiation of neurons into various sub-types, adding complexity and versatility to brain function (Bollimuntha et al. 2017). Intracellular Ca^{2+} concentration is stringently maintained at low resting levels of 50-200 nM in mammals and most other vertebrates (Capiod et al. 1989; Johnson et al. 1997) or 200-300 nM in marine molluscs (Baker et al. 1971; Fisher et al. 1994). This tightly controlled, low concentration of Ca^{2+} is made possible by a complex array of check points in the form of ion channels, exchangers, and pumps found in both the plasma membrane and the membrane of intracellular organelles such as the endoplasmic reticulum, Golgi apparatus, mitochondria, and to some extent, the nucleus (Brini et al. 2014). As such, Ca^{2+} signals are often a short-lived, transient increase in cytosolic concentration of a specific magnitude, so as to affect an array of intended Ca^{2+}-sensitive proteins (Berridge 1998; Van Haasteren et al. 1999).

Ca^{2+} typically exerts an effect by either binding directly to effector proteins, or by pairing with associated modulatory domains, such as the commonplace protein, calmodulin (CaM) (Ghosh and Greenberg 1995). One such example of this is the Ca^{2+}-mediated expression of the proto-oncogene *c-fos*. Ca^{2+} influx is able to induce *c-fos* expression via the Ca^{2+} response element (CRE), which is a sequence in the *c-fos* gene (Sheng et al. 1990). This is done via the phosphorylation of the CRE binding protein (CREB) by a Ca^{2+}-CaM-dependent protein kinase (Bartel et al. 1989; Deisseroth et al. 1998; Sheng et al. 1990).

Interestingly, many modulatory proteins, such as CaM, will form close and/or physical interactions with L-type Ca^{2+} channels, or other Ca^{2+} sources, in order to allow for an even more rapid and concerted regulatory response to a spike in free intracellular Ca^{2+} (Catterall 2011). Thus, in addition to acting on distant targets, Ca^{2+} influx can directly modulate excitability by interacting with ion channels at the membrane (Kramer and Zucker 1985). For example, Ca^{2+} is able to directly gate native non-selective cation channels, as well as certain transient receptor potential (TRP)-family cation channels (Knox et al. 1996; Liman 2003; Lupinsky and Magoski 2006; Zurborg et al. 2007). Ca^{2+} also opens certain K^+ channels, which are abundant in the nerve terminal and cause hyperpolarization following Ca^{2+} influx, effectively terminating neurotransmission (Marrion and Tavalin 1998; McManus 1991; Robitaille et al. 1993).

Voltage-gated Ca^{2+} channels

Voltage-gated Ca^{2+} channels are a diverse family of multi-subunit complexes that enable Ca^{2+} ions to traverse the plasma membrane following a depolarization of the membrane potential (Ahlijanian et al. 1990; Catterall 2011; Moore and Murphy 2020). Commonly found in skeletal, smooth, and cardiac muscle cells, in addition to neurons, these channels are made up of α1, α2, β, δ, and γ subunits with varying structures based on cell type (Bers 2002; Catterall 2011; Tanabe et al. 1993; Tsien et al. 1988). The typical voltage-gated Ca^{2+} channel is comprised of a pore forming subunit (α1) as well as several additional subunits (α2δ, and β). The α1 pore forming subunit is ~200 kD and organized into 4 repeating transmembrane domains, each with 6 segments. The C-terminal domain contains regions (EF-hand and IQ motifs) essential for Ca^{2+}-dependent regulation of the channel and certain protein-protein interaction (**Fig. 1**) (Ames 2021; Zamponi et al. 1997). Both the β & δ subunits play an integral role in trafficking the channels to the plasma membrane and regulating the voltage dependence. Additionally, modulation by other

Fig 1

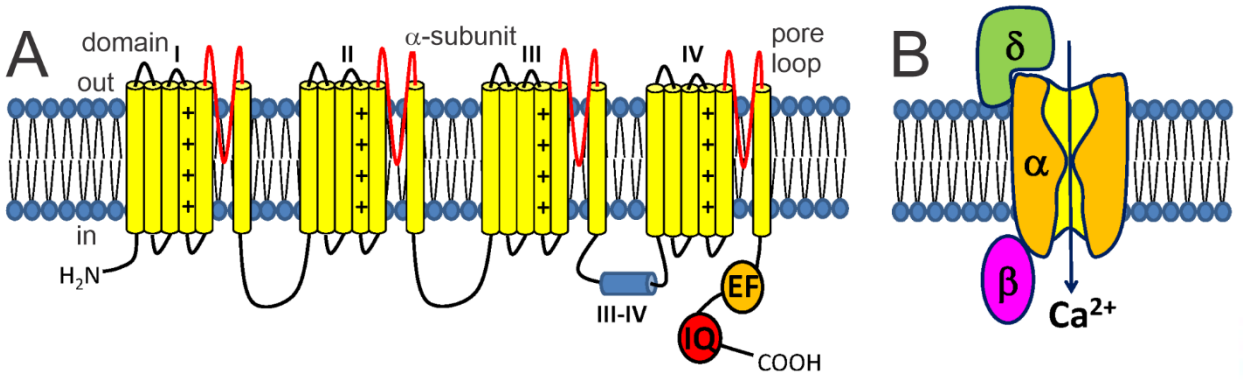

Figure 1. L-type Ca^{2+} channel structure.

A, The α-subunit consists of 4 transmembrane domains (I-IV) that contain 6 helices (*yellow*) and a pore loop (*red*). The III-IV linker is the VDI gate. The cytosolic C-terminal domain is comprised of an EF-hand domain (*orange*) and IQ-motif (*red*). **B,** The L-type channel is composed of pore-forming α-subunit with associated β- and δ-subunits. Modified from Ames (2021).

proteins and signalling molecules occurs frequently via the β subunit (Arikkath and Campbell 2003; Dolphin 2016; Moore and Murphy 2020). Isolation of voltage-gated Ca^{2+} channels from neurons showed that, unlike those found in muscle cells, the neuronal Ca^{2+} channels consisted of α1, α2δ, and β subunits but no γ subunit (Ahlijanian et al. 1990; Chang and Hoseys 1988).

Ca^{2+} channels can be categorized into 3 distinct families, based on the genes which encode them: Ca_v1 (L-type, long-lasting), Ca_v2 (P-type, Purkinje; N-type, neural; R-type, resistant to block) and Ca_v3 (T-type, transient), which in general, are also distinguishable by their functional and pharmacological attributes (Ertel et al. 2000; Lipscombe et al. 2004). The L-type Ca^{2+} channels are so named for their "long-lasting" Ca^{2+} currents that show limited steady-state inactivation during depolarization, which make them key regulators of neuronal excitability and synaptic transmission (Ames 2021; Catterall 2011; Tsien et al. 1988). Although much of the literature on Ca^{2+} channels focuses on vertebrates, homologues of Ca_v1, Ca_v2, and Ca_v3 have been identified in various invertebrate species, including molluscs (Spafford et al. 2006; White and Kaczmarek 1997). However, invertebrate channels are less reliably identified by the pharmacological means commonly used in vertebrates, but instead are frequently distinguished by electrophysiological properties (Kits and Mansvelder 1996).

Ca^{2+} dependent inactivation of the Ca^{2+} channel

The inactivation of ion channels is essential to the control of both excitability and the levels of intracellular Ca^{2+}. For voltage-gated Ca^{2+} channels, inactivation is mediated by two processes: Ca^{2+}-dependent inactivation (CDI) and voltage-dependent inactivation (VDI) (Cens et al. 2006; Stotz and Zamponi 2001). VDI is common to all voltage-gated Ca^{2+} subtypes; however, the exact mechanistic basis of this form of inactivation is not entirely clear. One model proposes that the S6 segment in the α1 subunit experiences a conformational change in response to

prolonged depolarization – this structural rearrangement exposes a docking site, which in turn allows the intracellular linker between domains I-II to act as a hinge-lid-like gate, blocking the pore in a voltage-dependent manner (Simms and Zamponi 2014). Ca^{2+} entry is also governed by CDI, which was first discovered in *Paramecium* and subsequently confirmed in *Aplysia* neurons (Brehm and Eckert 1978; Tillotson 1979) and then vertebrate neurons (Akaike et al. 1988). Contrary to the canonical notion that rapid gating of ion channels can only be initiated by transmembrane voltage, CDI is capable of quickly turning off Ca^{2+} channels and is totally dependent on CaM (Ben-Johny and Yue 2014; Simms and Zamponi 2014).

For many voltage-gated Ca^{2+} channels, including L-type channels, the Ca^{2+}-sensing protein, CaM, is pre-associated with the C-terminus, via an EF-hand region or Isoleucine-Glutamate domain on the channel (Ben-Johny and Yue 2014; Simms and Zamponi 2014). Ca^{2+} enters the cell and binds CaM, which turns off the channel in a direct, negative feedback pathway (Guerini 1997; Lee et al. 1999). In addition, Ca^{2+} can bind free cytosolic CaM and then activate the protein phosphatase, calcineurin, which effectively inhibits the channel by dephosphorylation (eg, at serine 1928 in mammalian $Ca_v1.2$) (Hell et al. 1993; Zühlke et al. 1999). Collectively, these processes lead to a faster rate of inactivation due to both CDI as well as cumulative VDI.

Neurosecretion

One of the most essential roles of Ca^{2+} is the promotion of neurosecretion, ie, the release of neurotransmitters. Secretion is triggered by a rise in intracellular Ca^{2+}, and the extent of secretion is largely dependent on the degree of Ca^{2+} influx (Dodge and Rahamimoff 1967; Katz and Miledi 1967). Classical neurotransmitters are produced in nerve terminals and packaged into small, clear vesicles (40-60 nm), that are stored until release (Purves et al. 2001). In contrast, neuropeptides and hormones are principally synthesized in the soma (Purves et al. 2001). For

peptides, larger pre-propeptides are first translated and then undergo an initial cleavage in the rough endoplasmic reticulum, where they are then packed into synaptic vesicles in the Golgi complex as propeptides (Brownstein et al. 1980; Purves et al. 2001). The final cleaving of propeptides occurs within the vesicle as it travels down the axon to the terminal, or in some instances to the dendrites or adjacent somatic membrane, to await secretion (Brownstein et al., 1980; Purves et al., 2001).

Transmitters are released at the terminal when the vesicular and the plasma membrane fuse (Südhof 2012). Fusion takes place through the physical interaction of SNARE (soluble N-ethylmaleimide-sensitive factor attachment protein receptors) complex proteins syntaxin-1 and synaptosome-associated-protein of 25-kDa (SNAP-25), which are bound to the plasma membrane, and synaptotagmin-1, which is bound to the vesicular membrane (Jahn and Scheller 2006; de Wit 2010). Secretion is mediated by synaptotagmin acting as the Ca^{2+} sensor (Meinrenken et al. 2003), where Ca^{2+} binds via an aspartate residue on the C2-domain (Coussens et al. 1986; Von Poser et al. 1997). The binding of Ca^{2+} allows for synaptotagmin to interact with the SNARE-complex and membrane phospholipids (Fernández-Chacón et al. 2001; Pang et al. 2006; Südhof 2012), which then form a pore to expel the transmitter into the synaptic cleft (Chapman 2002; Rettig and Neher 2002). In general, only a small fraction of docked vesicles fuse and release their contents after Ca^{2+} influx, suggesting that the rate limiting component of release is the magnitude of Ca^{2+} influx rather than the availability of release competent vesicles (Wadel et al. 2007; de Wit 2010).

Remarkably, Ca^{2+} influx to vesicle fusion and transmitter release happens in as little as 100 μs for classical transmitters, which is faster than most neuronal action potentials (Sabatini and Regehr 1996). This is possible as the vesicles and voltage-gated Ca^{2+} channels co-localize in

the axon terminal (Bennett 1997; Stanley 1993). Although the secretion of hormones and neuropeptides utilizes machinery similar to classical neurotransmitters, these vesicles do not co-localize, or co-localize to a lesser extent, with Ca^{2+} channels, and thus require a larger amount of Ca^{2+} for secretion (Bicknell 1988; Bicknell and Leng 1981; Peng and Horn 1991; Whim et al. 1997). Many neuroendocrine cells, from both vertebrates and invertebrates, overcome this larger Ca^{2+}obligation by enhancing the Ca^{2+} current via a PKC mediated pathway (Groten and Magoski 2015; Swartz et al. 1993; Zamponi et al. 1997). For example, in *Aplysia* bag cell neurons, PKC induces the recruitment of covert Ca^{2+} channels for insertion into the membrane, resulting in a substantially greater Ca^{2+} influx and secretory output (Groten and Magoski 2015). The surplus Ca^{2+} influx also increases Ca^{2+}-induce Ca^{2+} release (CICR) from mitochondria (Geiger and Magoski 2009), which act in concert to prolong neuropeptide release (Groten and Magoski 2015).

Aplysia californica as a model of neurosecretion and Ca^{2+} handling

My goal is to understand the role of Ca^{2+} handling in controlling Ca^{2+} channels from neuroendocrine cells. In this context, I employed the tractable model *Aplysia californica* (**Fig. 2 A**). *Aplysia* is a shell-less sea snail with a well-defined nervous system; pertinent to this work, are the bag cell neurons, a group of extensively studied neuroendocrine cells that control reproductive behaviour (Frazier et al. 1967; Kupfermann and Kandel 1970) (**Fig. 2 B**). Bag cell neurons are found in two discrete clusters, each containing 200-300 cells, rostral to the abdominal ganglion (**Fig. 2 A, C**). These cells sit at a quiescent membrane potential of ~ -60 mV, but upon brief cholinergic synaptic input from higher brain regions, enter a sustained (~30 min) period of activity, termed the afterdischarge (Frazier et al. 1967) (**Fig. 3 A**). This sustained burst of firing is synchronous between cells, owing to them being electrically coupled via gap

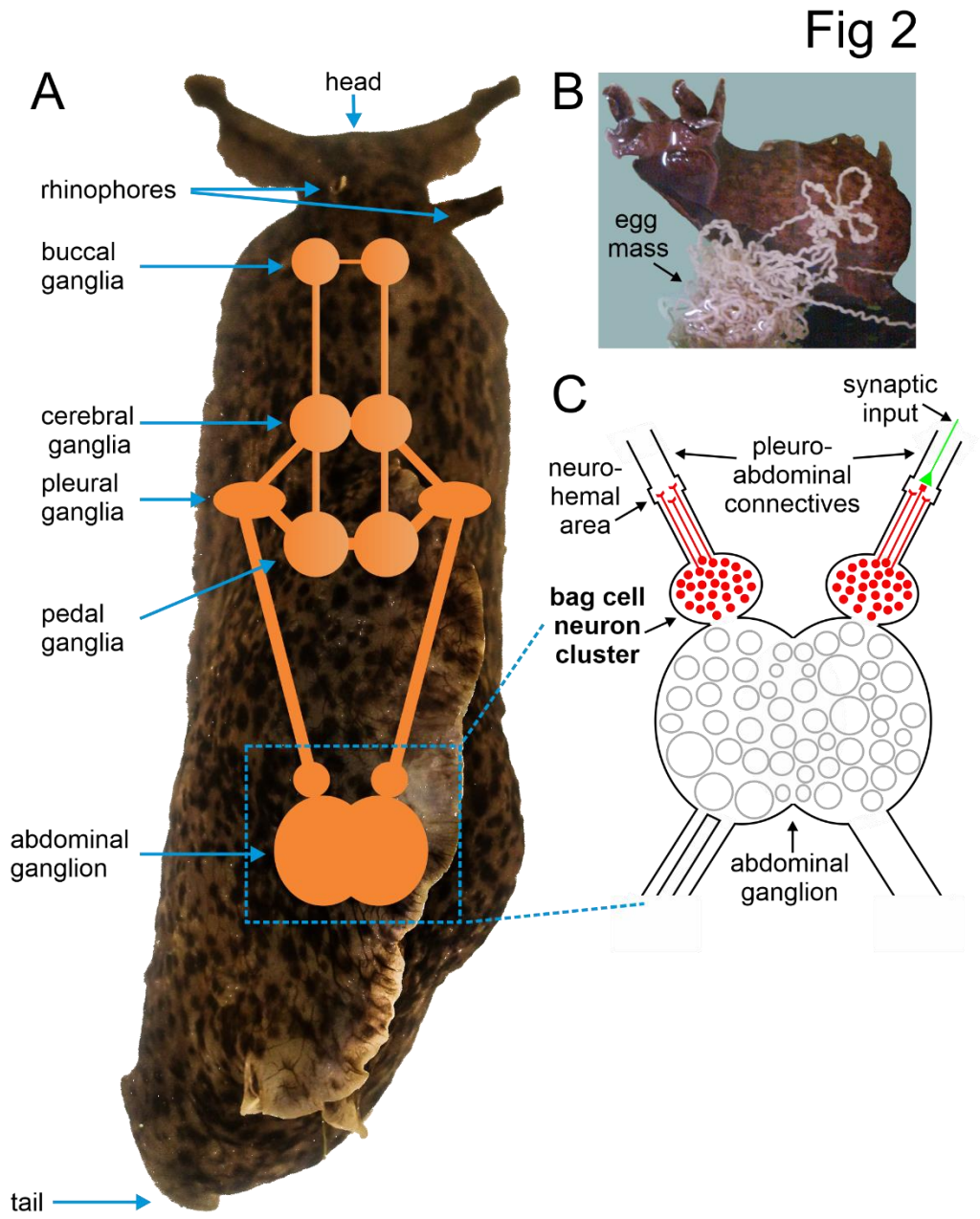

Figure 2. Representative *Aplysia* nervous system and bag cell neuron anatomy (dorsal view).

A, The *Aplysia* central nervous system is made up of paired buccal, cerebral, pedal, and plural ganglia, along with a single abdominal ganglion (shown ~10 times life-size). **B,** The snail is usually ~15 cm in length and ~5 cm across. As the final act of reproduction, it lays a string-like mass of fertilized eggs. **C,** The two bag cell neuron clusters (*red*) are at the rostral end of the abdominal ganglia. The neurons extend processes for secretion (*fletched endings*) to a neurohemal area where peptides are released into the bloodstream or to receive (*boxed ending*) descending synaptic input (*green triangle*). A-C, Modified from Sturgeon et al. (2018).

Fig 3

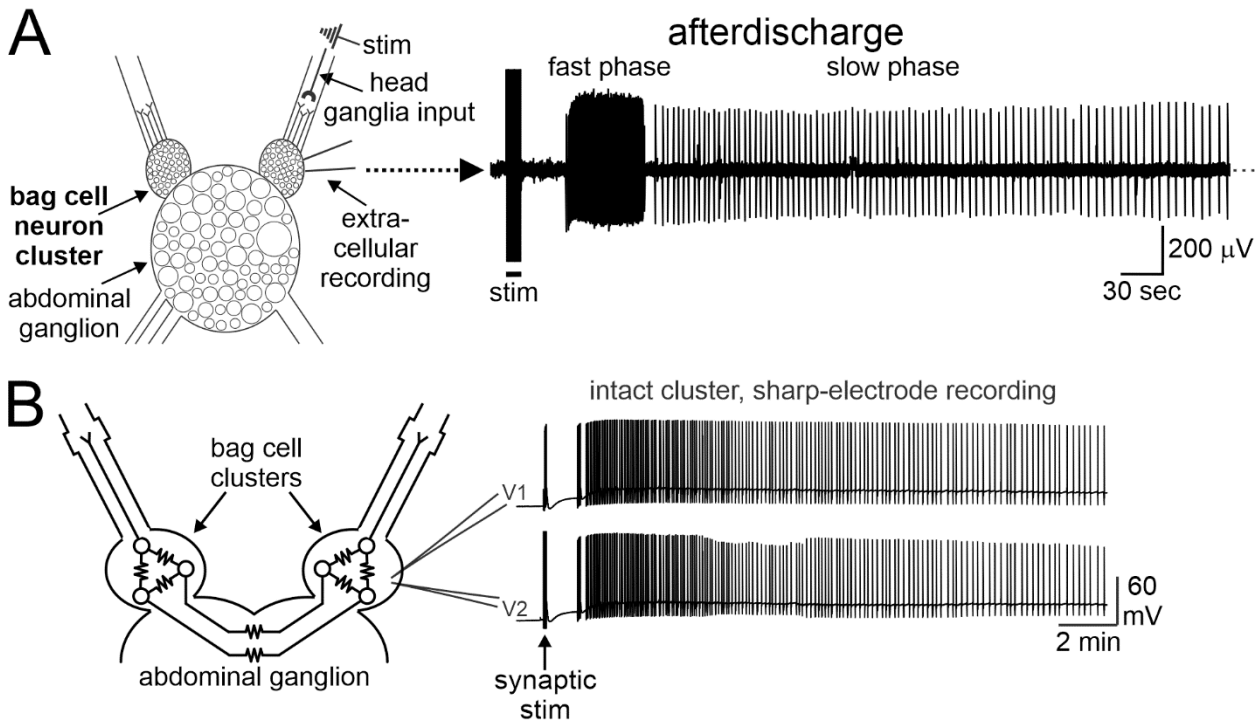

Figure 3. Bag cell neuron afterdischarge and electrical coupling.

A, Line-drawing of the abdominal ganglion depicting how the extracellular recording electrode is placed over one bag cell neuron cluster, along with the stimulating electrode on the descending synaptic afferents (*left*). A transient synaptic stimulus (stim, at *bar*) to the cluster evokes an afterdischarge, with typical fast- and slow-phase firing (*right*); each deflection represents the activity of all neurons in the cluster. Recording from Magoski unpublished. **B,** Diagram of both intra- and inter-cluster electrical coupling between bag cell neurons (*left*). Sharp electrodes are inserted into two neurons within a single cluster. The membrane potential recordings (*right*) reveal synchronous firing between the cells once an afterdischarge is elicited following stimulation (at *arrow*). Modified from Dargaei et al. (2014).

junctions (Dargaei et al. 2014; Kaczmarek et al. 1979) (**Fig. 3 B**). Throughout the duration of the afterdischarge, a 36-amino acid neuropeptide, known as egg-laying hormone (ELH) is released into the blood stream at a neurohemal area adjacent to the clusters (Arch 1972; Chiu et al. 1979). ELH results in a series of behavioural changes in the animal, culminating in the deposition of fertilized eggs (Arch 1972; Pinsker and Edward Dudek 1977) (**again see Fig. 2 B**).

The afterdischarge begins with an ~1 min fast-phase of ~5 Hz firing, followed by a more prolonged ~30 min slow-phase of ~1 Hz firing (Fisher et al. 1994; Kaczmarek et al. 1982) (**again, see Fig. 3 A**). During the fast-phase, Ca^{2+} enters through the voltage-gated Ca^{2+} channel, Apl Ca_v1 (Acosta-Urquidi and Dudek 1981; White and Kaczmarek 1997; Woolum and Strumwasser 1988; Zhang et al. 2008). This initial Ca^{2+} influx is dispersed throughout the cell, where it exerts its numerous effects. One such effect is CICR, from both the endoplasmic reticulum, via ryanodine receptors, which are essentially Ca^{2+}-activated Ca^{2+} channels, and from the mitochondria, where Ca^{2+} is taken up by the mitochondrial Ca^{2+} uniporter (MCU) and then released via Na^+/H^+-Ca^{2+} exchangers (Fisher et al. 1994; Geiger and Magoski 2008; Groten et al. 2016). CICR has been observed in neurons of many species, both vertebrate and invertebrate (Geiger and Magoski 2008; Lee et al. 2007; Lipscombe et al. 1988; Neering and McBurney 1984; Richter et al. 2005; Werth and Thayer 1994). The subsequent prolonged Ca^{2+} elevation from CICR likely contributes to ongoing neuropeptide secretion (Groten and Magoski 2015), potentially via Ca^{2+}-Syt-SNARE complex interactions (Fernández-Chacón et al. 2001; Pang et al. 2006; Südhof 2012). Phospholipase C is also activated, potentially by Ca^{2+} or voltage (Thore et al. 2005), and by breaking down phosphatidylinositol 4,5-bisphosphate, it generates IP_3 and diacyglycerol; the latter activates PKC, which then acts as a downstream effector of Ca^{2+} influx (Wayne et al. 1999).

Free cytosolic Ca^{2+} is dynamically controlled by vairous of plasma membrane or organelle channels, pumps, and exchangers. With respect to Ca^{2+} removal, this includes the plasma membrane Ca^{2+}-ATPase (PMCA), the plasma membrane Na^{+}/Ca^{2+}-exchanger, the endoplasmic reticulum Ca^{2+}-ATPase (SERCA) and the MCU (Groten et al. 2013) (**Fig. 4**). In bag cell neurons, voltage-gated Ca^{2+} influx removal is controlled by the MCU and the PMCA, with little-to-no contribution from the Na^{+}/Ca^{2+}-exchanger or SERCA (Geiger and Magoski 2008; Groten et al. 2013, 2016). Additionally, it has been demonstrated that blocking Ca^{2+} extrusion systems can influence the contribution of the mitochondria to intracellular Ca^{2+} dynamics. Groten et al. (2016) showed that inhibiting the PMCA using carboxyeosin increased the extent of CICR by increasing mitochondrial loading. In turn, CICR was drastically reduced by blocking Na^{+}-Ca^{2+} or H^{+}-Ca^{2+} exchangers on the mitochondria with tetraphenylphosphonium chloride (TPP) (Groten et al. 2013; Groten et al. 2016) Interestingly, blocking the PMCA did not affect endoplasmic reticulum dependent Ca^{2+} dynamics in a similar manner (Groten et al. 2016).

One implication of these Ca^{2+} removal systems, which is not well understood, is any potential effect on the CDI of the voltage-gated Ca^{2+} channel. Preliminary data from Groten (2015) revealed that repetitive opening of the bag cell neuron Ca^{2+} channel, using a 5-Hz, 1-min train stimulus of square pulses, lead to modest, but clear use-dependent run-down – ostensibly CDI (**Fig. 5**). Moreover, in the presence of carbonyl cyanide 4-(trifluoromethoxy) phenylhydrazone (FCCP), which collapses the mitochondrial membrane potential, and prevents Ca^{2+} uptake, the same train stimulus resulted in far greater run-down. Groten and Magoski (2015) also demonstrated that the mitochondria sequestered Ca^{2+} from a train stimulus by measuring the cytosolic Ca^{2+} concentration using the Ca^{2+}-sensitive dye, fura-PE3. In particular, FCCP caused a sharp rise in Ca^{2+} concentration, due to the elimination of mitochondrial voltage resulting in Ca^{2+}

Fig 4

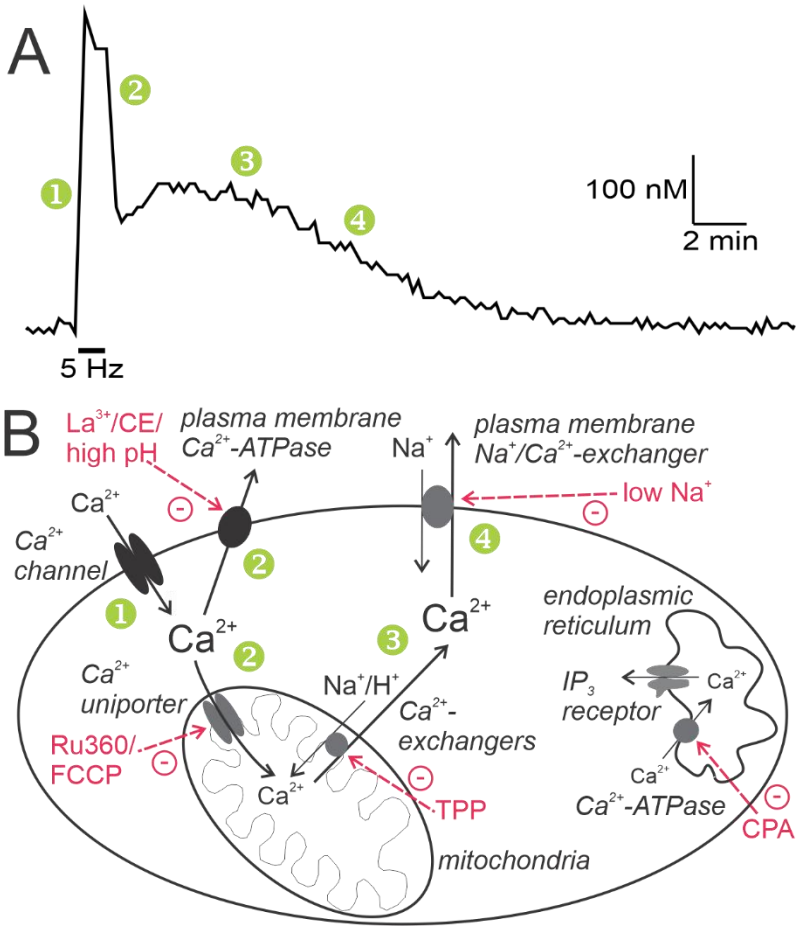

Figure 4. Ca^{2+} handling in the bag cell neurons.

A, Time course changes to intracellular Ca^{2+} of a cultured bag cell neuron following a 5-Hz, 60-sec train-stimulus (*at bar*) of voltage steps (75-ms pulses, from -80 to 0 mV). Ca^{2+} imaged by exciting fura at 340 nm and 380 nm, then taking the ratio of light emitted through a 510 nm barrier filter. Numbers correspond to events outlined in panel *B*. Based on Geiger and Magoski, (2008); Groten et al. (2013). ***B,*** Cellular mechanisms of Ca^{2+} handling: **1:** Ca^{2+} enters through the voltage-gated Ca^{2+} channels opened by stimulation. **2:** Ca^{2+} is taken up mainly via the mitochondrial Ca^{2+} uniporter, which can be antagonized directly with Ru360 or prevented with FCCP. Ca^{2+} is also removed by the plasma membrane Ca^{2+}-ATPase, which can be blocked by La^{3+}, CE or high extracellular pH. **3:** sequestered Ca^{2+} is released back into the cytosol by mitochondrial Na^{+}-Ca^{2+} or H^{+}-Ca^{2+} exchangers, which can be stopped by TPP. **4:** the released Ca^{2+} is removed from the cytosol by the plasma membrane Na^{+}-Ca^{2+} exchanger, which can be prevented by the removal of extracellular Na^{+}. Although bag cell neurons contain endoplasmic reticulum with IP_3 receptors and a Ca^{2+}-ATPase, which can be blocked by CPA, they do not handle voltage-gated Ca^{2+} entry. (Courtesy of Dr. NS Magoski)

Fig 5

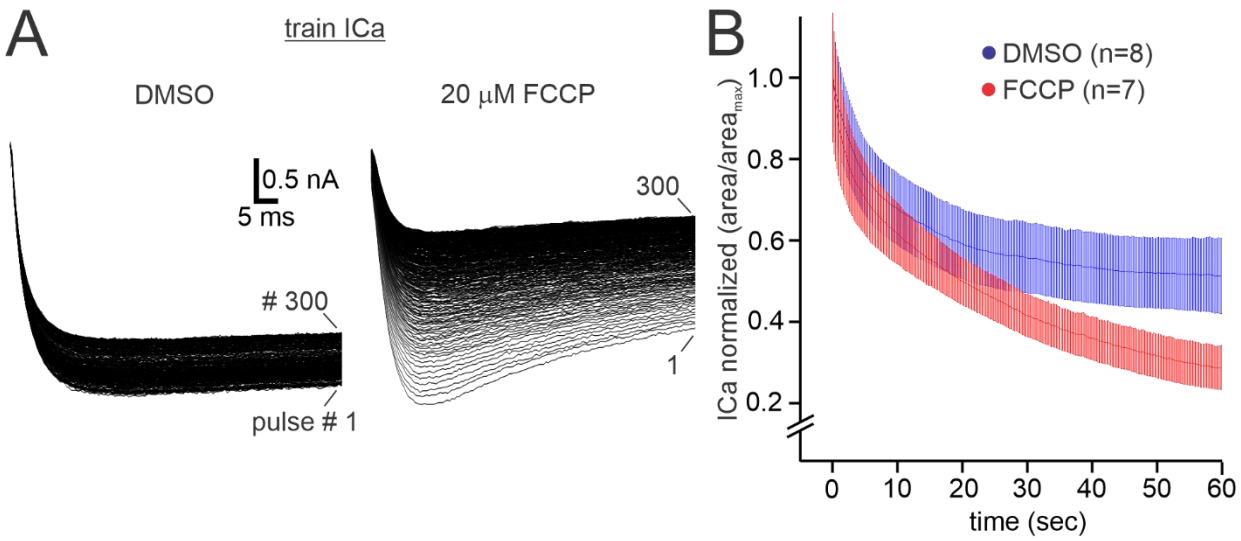

Figure 5. Ca^{2+} current rundown is increased in the presence of FCCP.

A, *Left*, Ca^{2+} currents measured from a neuron given DMSO and stimulated with a 5-Hz, 1-min train-stimulus of 75-ms depolarizing steps under whole-cell voltage-clamp. The shifting band of traces is due to use-dependent inactivation. With mitochondrial Ca^{2+} uptake, functional, use-dependent inactivation occurs at a moderate rate. All sweeps are overlaid and the first and last traces are indicated. *Right*, in a separate neuron treated with 20 μM FCCP to prevent mitochondrial Ca^{2+} uptake, the rundown during the train is more prominent than in DMSO, as indicated by the small Ca^{2+} current magnitude at the last pulse. **B**, Summary data presenting the normalized Ca^{2+} current magnitude for each pulse of the train-stimulus in DMSO and FCCP. DMSO-treated cells (*blue*) rundown to ~50% of the maximum value during the train while those in FCCP (*red*) end at ~30% of maximum. Modified from Groten (2015).

Fig 6

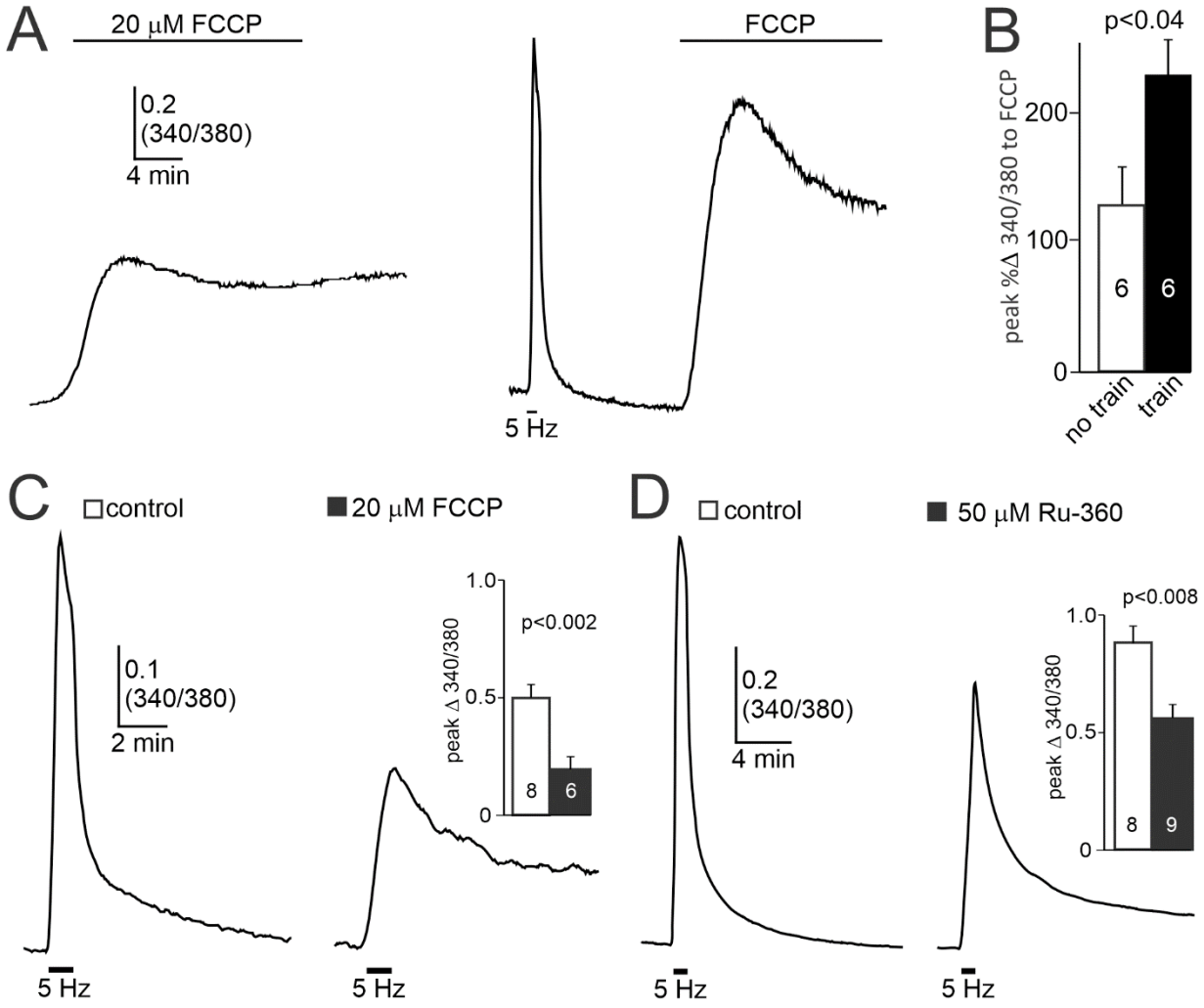

Figure 6. FCCP-induced rise in intracellular Ca^{2+} is mitigated by Ru360.

A, *Left*, FCCP causes intracellular Ca^{2+} release by collapsing the mitochondrial membrane potential. *Right*, After a large influx of Ca^{2+} from a 5-Hz, 1-min train of 75-ms depolarizing pulses, the FCCP-induced Ca^{2+} release is greater. 5 mM EGTA was included in all recordings to prevent CICR. **B,** Delivering the train-stimulus before FCCP significantly enhances the response to FCCP. **C,** *Left*, In a DMSO-treated neuron, the stimulus-train evokes a substantial Ca^{2+} influx, followed by rapid a recovery. *Right*, In a neuron exposed to FCCP, to prevent mitochondrial Ca^{2+} uptake, the stimulus-train elicits a comparatively small Ca^{2+} influx with a slow recovery. *Inset*, FCCP significantly reduces the train-stimulus Ca^{2+} influx compared to DMSO control. **D,** Relative to control (*left*), Ca^{2+} transients to the train-stimulus are markedly smaller in the presence of intracellular Ru360 (*right*), a blocker of the MCU. *Inset*, Ru360 significantly reduces the change in Ca^{2+} influx during the train-stimulus. A and B, Moified from Groten et al. (2013); C and D, Modified from Groten (2015).

leaking out of the organelle. This was significantly increased by loading the mitochondria with Ca^{2+} using a 5-Hz, 1-min train-stimulus of depolarizing steps prior to administering FCCP (**Fig. 6 A, B**). Consistent with mitochondria acting as a potential determinant for CDI, both FCCP and the MCU blocker, Ru360, significantly mitigated the train-stimulus-induced rise in intracellular Ca^{2+} (**Fig. 6 C, D**).

Overall, the role of the PMCA and the MCU in Ca^{2+} dynamics opens up the possibility that these systems may have a role in Ca^{2+}-mediated processes. As such, I will test the hypothesis that *intracellular Ca^{2+} handling, by both membrane transport and organelles, controls Ca^{2+} channel inactivation*. The data presented here show that Ca^{2+} influx and intracellular Ca^{2+} dynamics are heavily influenced by Ca^{2+} handling proteins and Ca^{2+} reservoirs. The result is a profound impact on current inactivation, with implications for endo/exocytosis.

Chapter 2 - Materials and Methods

Animals and cell culture

Adult *Aplysia californica* (a hermaphrodite) weighing 150-500 g were obtained from Marinus (Long Beach, CA). Animals were housed in an ~300-L aquarium containing continuously circulating, aerated artificial sea water (Instant Ocean; Aquarium Systems, Mentor, OH) at 16-18°C on a 12/12-hr light/dark cycle and fed Romaine lettuce 5 times/wk. For primary cultures of isolated bag cell neurons, animals were anesthetized by an injection of isotonic $MgCl_2$ (~50% body weight), the abdominal ganglion removed, and incubated for 18 hr at 22°C in Dispase II (13.33 mg/ml; 4942078001; Roche/Sigma-Aldrich; Oakville, ON) dissolved in tissue culture artificial sea water (tcASW) (composition in mM: 460 NaCl, 10.4 KCl, 11 $CaCl_2$, 55 $MgCl_2$, 15 4-(2-hydroxyethyl)-1-piperazineethanesulfonic acid (HEPES), 1 mg/ml glucose, 100 U/ml penicillin, and 0.1 mg/ml streptomycin, pH 7.8 with NaOH). The ganglion was then transferred to fresh tcASW and the bag cell neuron clusters dissected from the surrounding connective tissue. Using a fire-polished Pasteur pipette and gentle trituration, neurons were dispersed onto 35 x 10 mm polystyrene tissue culture dishes (353001/08772A; Falcon-Corning/Fisher Scientific, Ottawa, ON) filled with 2 ml of tcASW. Cultures were maintained in tcASW in a 14°C incubator and used within 1-3 d. Salts were obtained from Fisher Scientific or Sigma-Aldrich.

Whole-cell, voltage-clamp recording

Voltage-clamp recordings were made using an EPC-8 amplifier (HEKA Electronik/Harvard Biosciences, St-Laurent, QC) and the tight-seal, whole-cell method. Microelectrodes were pulled from 1.5-mm external, 1.2-mm internal-diameter borosilicate glass capillaries (TW150F-4; World Precision Instruments; Sarasota, FL) and had a resistance of 1-2 MΩ when filled with intracellular saline (see next paragraph). For recording Ca^{2+} currents,

pipette junction potentials were nulled, and pipette capacitive currents (4-7 pF) were cancelled prior to seal formation. Following break-through, the series resistance (2-5 MΩ) was compensated to 70-80% while the neuronal capacitance (300-900 pF) was cancelled. Current was filtered at 1 kHz by the EPC-8 built-in Bessel filter and sampled at 2 kHz using a Windows-based compatible personal computer, a Digidata 1550B analog-to-digital converter (Molecular Devices; Sunnyvale, CA), and the Clampex acquisition program of pClamp software (v10.2; Molecular Devices). Clampex was also used to set the holding and command potentials. Leak subtraction was typically performed in Clampex using a "P/4 protocol" from -60 mV with subpulses of opposite polarity and one-fourth the magnitude of a given test pulse, using a 500-ms subpulse interval and 500 ms before the test pulse. For measurements of Ca^{2+} current during a 5-Hz, 5-sec or 1-min train of depolarizing steps, leak current was measured by manually applying a single P/4 protocol, as described above, prior to the train. The leak currents were then subtracted off-line from the Ca^{2+} currents acquired during the train-stimulus and after the manual P/4 protocol. This technique was used because there was insufficient time between the depolarizing pulses of the train to run a recurring P/4 protocol.

Ca^{2+} current was isolated using Ca^{2+}-Cs^{+} -tetraethylammonium (TEA) ASW, as per tcASW, but with the NaCl and KCl replaced by TEA-Cl and CsCl, respectively, and the glucose and antibiotics omitted (composition in mM: 460 TEA-Cl, 10.4 CsCl, 55 $MgCl_2$, 11 $CaCl_2$, 15 HEPES, pH 7.8 with CsOH). In some cases, the $CaCl_2$ was replaced by equimolar amounts of $BaCl_2$ to measure the Ca^{2+}-dependent inactivation of the voltage-gated Ca^{2+} channel, while maintaining the electrochemical gradient. Whole-cell recordings used a Ca^{2+}-free Cs^{+}-aspartate-based intracellular saline (composition in mM: 70 CsCl, 10 HEPES, 11 glucose, 10 glutathione, 500 aspartic acid, 5 ATP (grade 2, disodium salt), and 0.1 GTP (type 3, disodium salt), pH 7.3

with CsOH). Certain experiments were performed with 20 mM of ethylene glycol-bis(β-aminoethyl ether)-N,N,N',N'-tetraacetic acid (EGTA) included in the internal saline. In other cases, the mitochondrial Ca^{2+} uniporter was blocked by adding the ruthenium amine complex, Ru360 (500 μM stock in intracellular saline; 50 μM final in pipette; 557440; Sigma-Aldrich), to the internal solution. To image Ca^{2+} (see next section) under whole-cell voltage-clamp, the intracellular saline was supplemented with 1 mM fura-PE3 (0110; Teflabs, Austin, TX) (Vorndran et al. 1995) to passively dye-fill neurons via the pipette.

Imaging of calcium

Most Ca^{2+} imaging was performed using cultured bag cell neurons plated on polystyrene tissue culture dishes (as per *Animals and cell culture*). However, in some cases Ca^{2+} was measured from cells plated onto glass coverslips (#1; 48366045; VWR; Chester, PA) coated with 1 μg/ml poly-L-lysine hydrobromide, (MW: 300,000; P1534; Sigma-Aldrich). Coverslips were glued with Sylgard silicone elastomer (SYLG184; World Precision Instruments) to holes drilled out of the bottom of the tissue culture dish. To perform Ca^{2+} imaging, neurons were filled with fura-PE3 under voltage-clamp in Ca^{2+}-Cs^{+} -TEA ASW for at least 30 min before recording, as described in the prior section.

All recordings were performed using a TS100-F inverted microscope (Nikon, Mississauga, ON) equipped with a Nikon Plan Fluor 20X objective (Numerical Aperture = 0.5). The light source was a 75-W Xe arc lamp and a multiwavelength DeltaRAM V monochromatic illuminator (Photon Technology International; London, ON) coupled to the microscope with a UV-grade liquid-light guide. Fura was excited at wavelengths of 340 and 380 nm. The excitation illumination was controlled by a shutter, which along with the excitation wavelength, was controlled by a Windows-based computer, a Photon Technology International computer interface,

and EasyRatio Pro software (v1.10; Photon Technology International). To allow for continuous Ca^{2+} image acquisition during experiments, the shutter usually remained open. Emitted light from fura was passed through a 400-nm long-pass dichroic mirror and a 480-550 nm emission barrier filter before being detected by a Photometrics Cool SNAP HQ2 charge-coupled device camera. The ratio of the emission following 340 and 380 nm excitation (340/380) was taken to reflect free intracellular Ca^{2+} (Grynkiewicz *et al*. 1985), and saved for subsequent analysis.

Most Ca^{2+} measurements were acquired from a somatic region of interest (ROI) at approximately the midpoint of the vertical focal plane and one-half to three-quarters of the cell diameter. Camera gain was maximized, pixel binning was set at 2, exposure time at each wavelength was fixed to ~1 sec, and images (696 x 520 pixels) were averaged 8 frames per acquisition.

Reagents and drug application

Solution exchanges were accomplished by manual perfusion using a calibrated transfer pipette to first exchange the bath (tissue culture dish) solution. In most cases where a drug was applied, a small volume (2-4 µl) of a concentrated stock solution (indicated below) was mixed with a larger volume of saline (~100 µl) that was initially removed from the bath, and this mixture was then pipetted back into the bath. Carboxyeosin (CE; 10 mM stock; C-22803; Invitrogen, Waltham, MA), and carbonyl cyanide 4-(trifluoromethoxy) phenylhydrazone (FCCP; 3 mM stock; 21857; Sigma-Aldrich) all required DMSO as a vehicle. The maximal final concentration of DMSO was 0.1-0.2% (v/v), which in control experiments as well as prior work from our laboratory, had no effect on membrane potential, various macroscopic or single channel current, resting intracellular Ca^{2+}, or Ca^{2+} transients evoked by action potentials (Lupinsky and

Magoski, 2006; Hung and Magoski, 2007; Gardam *et al*. 2008; Geiger and Magoski, 2008; Tam *et al*. 2009, 2011; Hickey *et al*. 2013).

Data analysis and statistics

Origin (v7.0; Originlab; Northhampton, MA) was used to import and plot ImageMaster Pro files as line graphs. Raw data was then transferred to Prism (v5; GraphPad Software, San Diego, CA) for analysis. Analysis of intracellular Ca^{2+} usually compared the steady-state value of the baseline 340/380 ratio with the ratio from regions that had reached a peak or new steady state during a response (340/380 peak – 340/380 baseline). Measurements of the baseline were determined by visually identifying the steady-state and averaging over a 1 min period, 10 sec prior to the response. Measurements of the peak were identified using the maximum value function in Excel (v16; Microsoft; Redmond, WA). Percent change of intracellular Ca^{2+} was calculated by determining the degree of Ca^{2+} release following a stimulus-induced change (340/380 peak – 340/380 pre-stimulus baseline 340/380) and dividing it by the 340/380 pre-stimulus baseline.

To quantify Ca^{2+} current magnitude, the peak current of each trace was measured in Clampfit, a program of pClamp. A pair of cursors, 8 ms apart, were placed 3 ms before current onset, and the average between these cursors taken as baseline. A second pair of cursors was placed on either side of the peak evoked current, and the peak was calculated as the difference between the baseline and absolute peak current. In some cases, data were normalized to cell size by dividing peak current values by whole-cell capacitance. The degree of Ca^{2+}-dependent inactivation of Ca^{2+} channels (Ca^{2+} current rundown) over the course of a train-stimulus (see *Results* for details) was calculated by measuring the peak change of the first induced current, and dividing the peak change of each subsequent current by that value. The Ca^{2+} current rundown

was expressed as a ratio of the initial induced current. Activation curves were produced by dividing the current elicited at each voltage step by the maximum current elicited during the protocol, typically +10 mV. This was averaged across cells at a given step voltage, plotted against that voltage, and fit with a Boltzmann equation in Prism. Activation and inactivation time constants were acquired by fitting mono-exponential decay functions to the activation and inactivation components of the Ca^{2+} current in Prism. The activation time period was defined as the time from the start of the inward current (immediately after the capacitance current) to the peak inward current. Conversely, the inactivation period was fitted to the range of time from the peak Ca^{2+} current to the last measurable point before the end of the depolarizing test pulse and the start of the capacitance artifact. For presentation, traces were selected that best represented the mean peak Ca^{2+} responses and, when necessary, aligned at the pre-stimulus baselines for each condition, regardless of their absolute baseline value.

Statistics were performed using Prism and Instat (v3.0; GraphPad Software). Summary data are presented as the mean ± standard error of the mean. The Kolmogorov-Smirnov method was used to test data sets for normality. If the data were normal, Student's unpaired t-test was used to test for differences between two means. To test for differences between multiple normally distributed means, an ordinary analysis of variance (ANOVA) with a Tukey-Kramer multiple comparisons test was used. Unless stated otherwise, all statistical comparisons between two means were two-tailed. Data were considered significantly different at $p<0.05$.

Chapter 3 - Results

One of the most essential roles of Ca^{2+} is the regulation and promotion of neurosecretion (ie, the release of neurotransmitters). The extent of secretion is largely dependent on the degree of Ca^{2+} influx (Dodge and Rahamimoff, 1967; Katz and Miledi, 1967). This Ca^{2+} entry is modulated by a process known as Ca^{2+}-dependent inactivation (CDI), first discovered in *Paramecium* and subsequently confirmed in *Aplysia* (Brehm and Eckert 1978; Tillotson 1979), then found to be universal in vertebrates (Simms and Zamponi 2014).

In order to confirm that cultured bag cell neuron voltage-gated Ca^{2+} current, ostensibly the Apl Ca_v1 channel, undergoes CDI, individual neurons were dissociated from the cluster for single cell recordings (**Fig. 7 D, *inset***). Experiments were performed in a Ca^{2+}-Cs^{+}-TEA-based extracellular solution, with a Cs^{+}-aspartate-based, EGTA-free, no added Ca^{2+} intracellular solution in the whole-cell pipette (see *Materials and Methods, Whole-cell, voltage-clamp recording* for details). TEA and Cs^{+} were used in place of Na^{+} and K^{+}, respectively, which effectively eliminated and Na^{+} current while also both serving to block K^{+} channels. These solutions allowed for the recording of isolated Ca^{2+} currents under whole-cell voltage-clamp. As EGTA is a Ca^{2+} chelating agent, recording without EGTA produced a more physiologically relevant environment, where Ca^{2+} was allowed to change dynamically.

The voltage-gated Ca^{2+} current in bag cell neurons undergoes Ca^{2+}-dependent inactivation

Ca^{2+} currents were evoked by 200-ms square pulses from a holding potential of -60 mV to +60 mV in 10-mV increments (n=11); this produced a classical U-shaped current-voltage curve seen in high-voltage-activated Ca^{2+} channels (**Fig. 7 A, B**). After normalizing these currents to the maximum evoked current and plotting against step voltage, channel activation was calculated using a

Fig 7

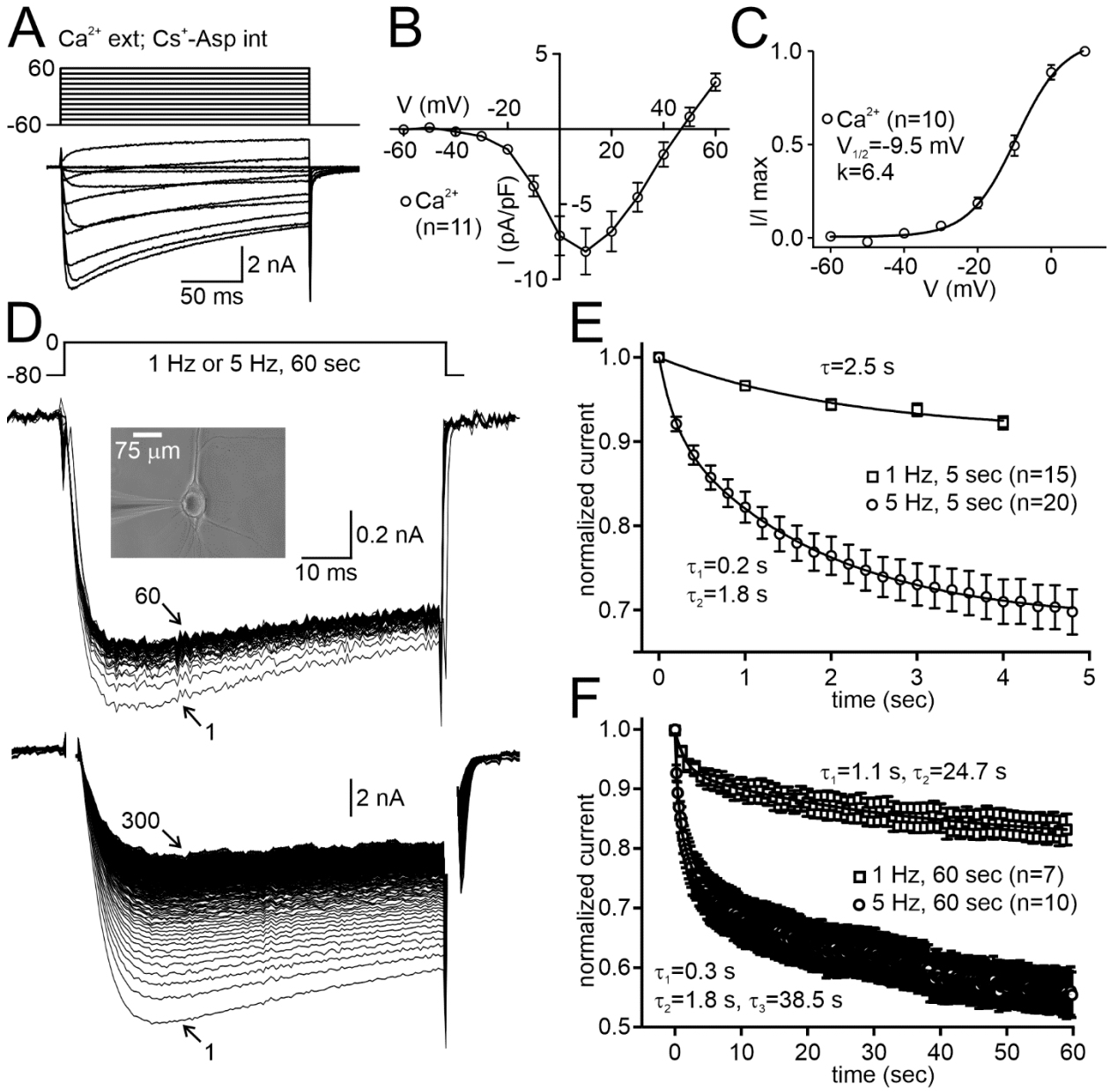

Figure 7. The voltage-gated Ca^{2+} channel undergoes Ca^{2+}-dependent inactivation.

A, Whole-cell voltage-clamp recordings of Ca^{2+} current evoked by 200-ms square pulses from -60 mV to +60 mV in 10-mV increments. Recordings were performed in Ca^{2+}-Cs^{+} -TEA ASW external solution, with Cs^{+}-aspartate-based intracellular saline. ***B,*** The mean I-V relationship of peak Ca^{2+} current density. ***C,*** Activation curve constructed by normalizing all currents to maximum current (at +10 mV) and plotting against test pulse voltage. The curve represents a fit with a Boltzmann function and provides a half-maximal activation voltage ($V_{0.5}$) and slope factor (k) of -9.5 mV and 6.4, respectively. ***D,*** Ca^{2+} current evoked from -80 mV with 75-ms pulses to 0 mV at 1 Hz (*top*) or 5 Hz (*bottom*) for 60 sec. All sweeps are overlaid and the first and last traces are indicated. Capacitance artifacts are omitted for clarity. Abscissa applied to both sets of traces.

Inset, A cultured bag cell neuron with recording pipette on the left. ***E***,***F***, Summary data presenting the mean current rundown during a 1-Hz or 5-Hz train-stimulus for 5-sec (*E*) or 60-sec (*F*). Current is normalized to the first sweep, and curves represent fits with mono, bi, or tri-exponential functions; time constants are shown adjacent.

Boltzmann fit. The mid-activation point of the Ca^{2+} current was -9.5 mV in control experiments, with a k of 6.4 (**Fig. 7 C**). The extent of Ca^{2+} current rundown was established using 75-ms square pulses to 0 mV at 1 Hz (n=15) or 5 Hz (n=20) for 5 sec, as well as 60 sec (n=7 and 10) (**Fig. 7 D**). These specific frequencies were used to emulate the fast- and slow-phase of the bag cell neuron afterdischarge (Fisher et al. 1994; Kaczmarek et al. 1982) (**Fig. 3 A**). Rundown was defined as the difference in evoked current between the first and each subsequent sweep; henceforth, rundown will refer to the difference between the first and final sweep. Ca^{2+} current rundown was more apparent both by increasing the duration and the frequency of the stimulus (**Fig. 7 E, F**). Specifically, over 5 sec the 1-Hz stimulus led to ~ 95% of the current remaining, while at 5 Hz, there was ~ 70% remaining. Over 60 sec, the 1-Hz train-stimulus resulted in ~ 85% of the current remaining, whereas at 5 Hz the remaining current was ~ 55%. This suggested that as the intracellular Ca^{2+} concentration rises, the extent of CDI becomes greater.

Ba^{2+}-based external solution reduces the extent of Ca^{2+}-current rundown

It is well-established that Ba^{2+} ions do not have a high affinity for Ca^{2+} effector proteins, such as calmodulin (CaM), despite being permeable through voltage-gated Ca^{2+} channels (Branchaw et al. 1997; Veselovskii and Fedulova 1986). As such, Ba^{2+} poorly binds to the channel-associated CaM and is thus unlikely to cause inactivation. I repeated the experiments outlined above, with the same intracellular solution, while swapping Ca^{+}-Cs^{+}-TEA for Ba^{2+}-Cs^{+}-TEA ASW as the extracellular solution. This resulted in a slightly smaller peak current during the 200-ms step protocol (n=11) when compared to the Ca^{2+} control (n=11), supporting that the ability of Ba^{2+} to pass through the channel was slightly less than that of Ca^{2+} (**Fig. 8 A, B**). Interestingly,

Fig 8

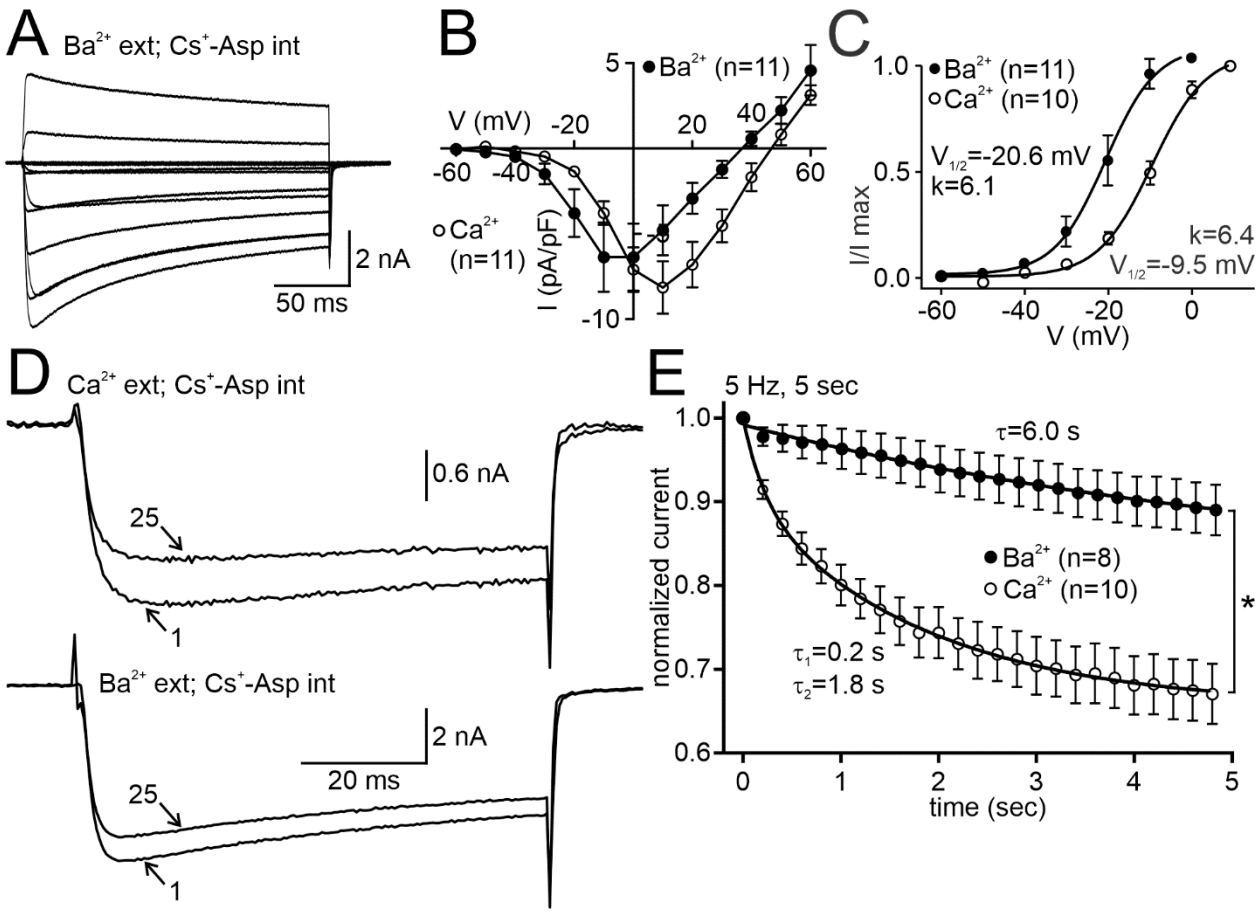

Figure 8. Ba^{2+}-based external solution reduces the extent of current rundown.

A, Whole-cell voltage-clamp recordings of Ba^{2+} current evoked by 200-ms pulses from -60 mV to +60 mV in 10-mV increments. ***B,*** The mean I-V relationship of peak Ba^{2+} current density is plotted with peak Ca^{2+} current density (reproduced from figure 4). ***C,*** Activation curves constructed by normalizing to maximum current (at +10 or 0 mV for Ca^{2+} and Ba^{2+}, respectively) and plotting against test voltage. The curves represent a fit with a Boltzmann function and provides a $V_{0.5}$ and k of -20.6 mV and 6.1, respectively for Ba^{2+}; these are right-shifted compared to Ca^{2+} current. ***D,*** Current with Ca^{2+} (*upper*; reproduced from figure 4) or Ba^{2+} as the charge carrier and evoked from -80 mV with 75-ms pulses to 0 mV at 5 Hz for 5 sec. First and last sweeps are overlaid and labeled. Abscissa applies to both sets of traces. ***E,*** Summary data presenting the mean current rundown during the 5-Hz, 5-sec stimulus-train in Ba^{2+}- and Ca^{2+}-based external saline. Current is normalized to the first sweep, and curves are fit with mono or bi-exponential functions. A comparison of the normalized current evoked by the final step of the train-stimulus shows that rundown is significantly more in Ca^{2+} (t_{28}=4.442; p=0.0001; unpaired Student's t-test).

when normalized to peak current and fit with a Boltzmann function, it was apparent that activation was at a more hyperpolarized voltage with Ba^{2+} as the charge carrier than control, with mid-activation points of $V_{1/2}$=-20.6 mV and $V_{1/2}$=-9.5 mV, respectively (**Fig. 8 C**). The k value was smaller in Ba^{2+} at 6.1, compared to the control k of 6.4. Moreover, current rundown was substantially reduced with Ba^{2+}. The rundown following a 5-Hz, 5-sec train-stimulus was ~9% in Ba^{2+} (n=8), compared to ~30% in Ca^{2+} control (n=10) (**Fig. 8 D, E**). This implied that rundown in the control condition was not simply use-dependent (also known as cumulative inactivation) but in fact depended, in part, on Ca^{2+} influx potentially interacting with the channel.

Buffering intracellular Ca^{2+} with EGTA reduces the extent of current rundown

Ethyleneglycol Bis(2-Aminoethyl Ether)-N,N,N',N' Tetraacetic Acid (EGTA) is a Ca^{2+} chelating agent that binds free Ca^{2+} with high affinity (pKa=11.00) (Al-Jobore and Roufogalis 1981). Further, EGTA is able to chelate Ca^{2+} nearly instantaneously when it enters the cell, and as such, free Ca^{2+} is presumably not able to interact with the channel (Zenisek et al. 2003). Subsequent experiments were performed with standard Ca^{+}-Cs^{+}-TEA ASW as the external solution, with Cs^{+}-aspartate internal solution containing 20 mM EGTA. Following the 200-ms protocol, Ca^{2+} currents evoked in the EGTA condition (n=9) achieved a slightly larger peak current when compared to the EGTA-free control (n=11) (**Fig. 9 A, B**). Similar to when Ba^{2+} was the charge carrier, the Ca^{2+} channel was activated at a more hyperpolarized voltage in the presence of EGTA than control (**Fig. 9 C**). Similarly, current rundown was reduced to ~91% remaining, by EGTA (n=9), substantially less than that of control (n=11) during the 5-Hz, 5-second train-stimulus (**Fig. 9 D, E**). This finding is in agreement with Ca^{2+} entry being necessary for rundown, but further suggests that free Ca^{2+} is required for CDI.

Fig 9

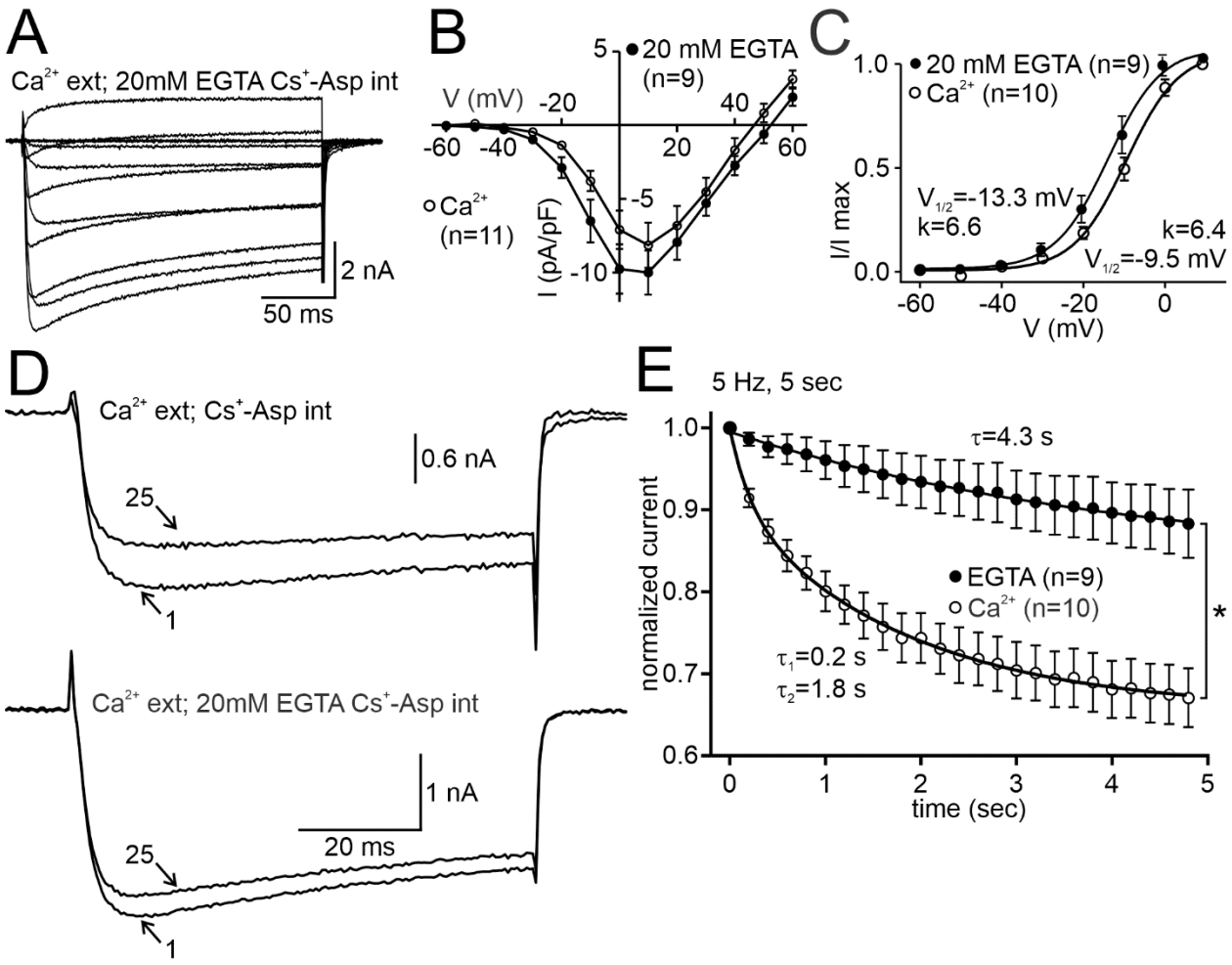

Figure 9. Buffering intracellular Ca^{2+} with EGTA reduces the extent of current rundown.

A, Whole-cell voltage-clamp recordings of Ca^{2+} current, in the presence of 20 mM EGTA, evoked by 200-ms pulses from -60 mV to +60 mV in 10-mV increments. Capacitance artifact removed for clarity. ***B,*** The mean I-V relationship of peak Ca^{2+} current density with EGTA is plotted with the EGTA-free Ca^{2+} current density (reproduced from figure 4). ***C,*** Activation curves constructed by normalizing to maximum current (at +10 mV) and plotting against test voltage. The curves represent a fit with a Boltzmann function and provides a $V_{0.5}$ and k of -13.3 mV and 6.6, respectively in EGTA, which is left-shifted compared to EGTA-free (reproduced from figure 4). ***D,*** Current evoked from -80 mV with 75-ms pulses to 0 mV at 5 Hz for 5 sec. First and last sweeps are overlaid and labeled. Abscissa applies to both sets of traces. ***E***, The mean current rundown during the train-stimulus for 20 mM EGTA and EGTA-free conditions. Current is normalized to the first sweep, and curves are fit with mono or bi-exponential functions. Comparison of the final step reveals that the current runs down significantly more in the EGTA-free condition (t_{28}=3.871; p=0.0006; unpaired Student's t-test).

Blockage of the mitochondrial calcium uniporter increases current rundown

The initial Ca^{2+} influx from the voltage-gated Ca^{2+} channel is handled (effectively buffered), among other means, by the mitochondria via the mitochondrial Ca^{2+} uniporter (MCU) (Geiger and Magoski 2008; Groten et al. 2013). I sought to establish the influence of mitochondrial buffering on CDI by blocking the MCU using 50 μM ruthenium 360 (Ru360), a potent and specific inhibitor of the MCU (Matlib et al. 1998; Zazueta et al. 1999) (**Fig. 4 B**). To do so, recordings were taken in Ca^{+}-Cs^{+}-TEA ASW external with Cs^{+}-aspartate internal solution containing 50 μM Ru360. The blocker was introduced into the neuron by whole-cell perfusion for 30 min prior to the start of the experiment. Again, following the voltage-step protocol, evoked Ca^{2+} currents reached an apparent larger peak in the Ru360 condition (n=10) when compared to control (n=11) (**Fig. 10 A, B**). Fitting the normalized data with a Boltzmann revealed a slight right-shift in the activation curve, with mid activation points of $V_{1/2}$=-6.8 mV and $V_{1/2}$=-9.5 mV for the Ru360 and control conditions, respectively (**Fig. 10 C**). Current rundown during the 5-Hz, 5-sec train stimulus was increased significantly by Ru360 (n=10), to ~58% of initial current, compared to the control rundown to ~70% remaining (**Fig. 10 D, E**). This further supports the notion that free cytosolic Ca^{2+} promotes CDI, and mitochondrial Ca^{2+} buffering plays a key role in controlling the amount of Ca^{2+}.

Inhibition of the plasma membrane Ca^{2+}-ATPase increases the extent of current rundown

It has also been previously demonstrated that blocking Ca^{2+} extrusion can influence the contribution of the mitochondria to intracellular Ca^{2+} dynamics (Groten et al. 2016). One such system, the plasma membrane Ca^{2+}-ATPase (PMCA), plays a primary role in the removal of voltage-gated Ca^{2+} influx (Groten et al. 2013). As such, I employed 10 μM of the PMCA inhibitor, carboxyeosin, to elucidate the role of Ca^{2+}-extrusion in CDI

Fig 10

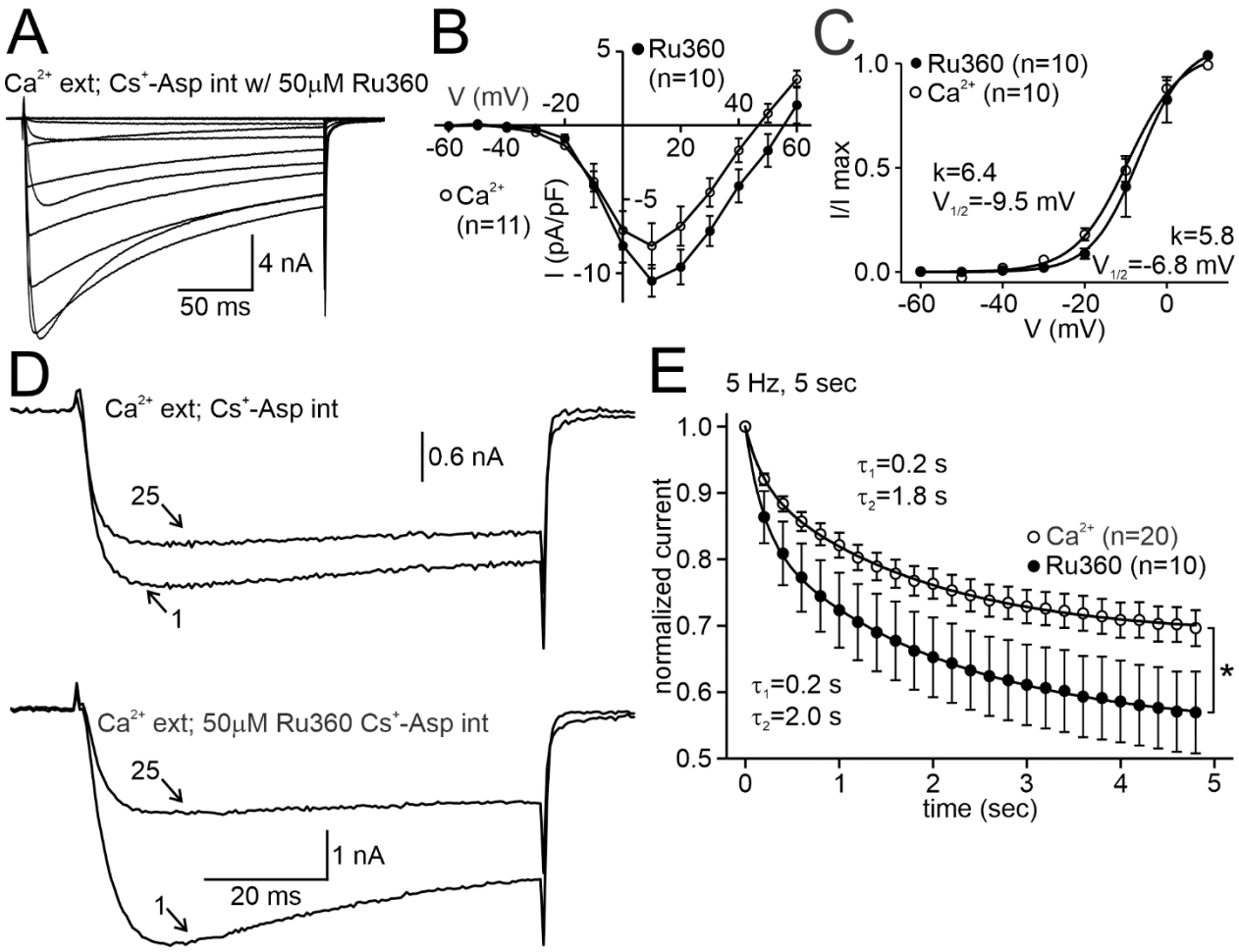

Figure 10. Blockage of the mitochondrial calcium uniporter increases current rundown.

A, Whole-cell voltage-clamp recordings of Ca^{2+} current, with 50 μM Ru360 in the intracellular solution, evoked by 200-ms pulses from -60 mV to +60 mV in 10-mV increments. ***B,*** The mean I-V relationship of peak Ca^{2+} current density in the presence of Ru360 is plotted with control Ca^{2+} current density (reproduced from figure 4). ***C,*** Activation curves constructed by normalizing to maximum current (at +10 mV) and plotting against test voltage. The curves represent a fit with a Boltzmann function and provides a $V_{0.5}$ and k of -6.8 mV and 5.8, respectively for the Ru360 condition, which is slightly right-shifted compared to control (reproduced from figure 4). ***D,*** Current evoked from -80 mV with 75-ms pulses to 0 mV at 5 Hz for 5 sec. First and last sweeps are overlaid and labeled. Abscissa applies to both sets of traces. ***E,*** The mean current rundown during the train-stimulus for Ru360 and control condition. Current is normalized to the first sweep, and curves are fit with a bi-exponential function. Comparing the current at the last step shows that rundown is significantly greater in the Ru360 condition (t_{26}=2.082; p=0.0473; unpaired Student's t-test).

(Gatto and Milanick 1993; Green et al. 1997). Experiments were performed in Ca^{+}-Cs^{+}-TEA ASW external with 10 μM carboxyeosin added to the bath for 10 min prior, and standard Cs^{+}-aspartate intracellular solution. Using the 200-ms step protocol, evoked Ca^{2+} currents reached a larger peak in the carboxyeosin condition (n=5) when compared to control (**Fig. 11 A, B**). A Boltzmann fit of the normalized data revealed a right shift in the activation curve, with mid activation points of $V_{1/2}$=-4.1 mV and $V_{1/2}$=-9.5 mV for the carboxyeosin and control, respectively (**Fig. 11 C**). Similar to Ru360, carboxyeosin (n=5) caused a significantly larger current rundown than control, with ~ 55% remaining, at the end of the 5-Hz 5-second train stimulus (**Fig. 11 D, E**). This bolsters the previous finding that Ca^{2+} extrusion via the PMCA influences intracellular Ca^{2+} dynamics.

Voltage-gated Ca^{2+} influx loads mitochondrial Ca^{2+} stores in an Ru360-sensitive manner

If the mitochondria are indeed acting as a sink for Ca^{2+} channel-mediated Ca^{2+} influx, then mitochondrial Ca^{2+} should increase following the train-stimulus and this should be prevented by Ru360. Neurons were loaded via the recording electrode with 1 mM of the Ca^{2+}-sensitive dye, fura-PE3 (Vorndran et al. 1995) in the Cs^{+}-aspartate internal solution, and mitochondrial Ca^{2+} content assessed by using carbonyl cyanide p-trifluoromethoxyphenylhydrazone (FCCP), a protonophore that collapses the mitochondrial membrane potential and results in passive leakage of Ca^{2+} out of the organelle into the cytoplasm (Groten et al. 2016; Heytler and Prichard 1962; Hickey et al. 2010). Under voltage-clamp at -60 mV, neurons were exposed to 3 μM FCCP without prior stimulation or following a 5-Hz 1-min train stimulus. In control conditions (n=5), there was a moderate increase of ~150% in cytosolic Ca^{2+} content following the introduction of FCCP (**Fig. 12 A, *left***). When the mitochondria were pre-loaded with the train-stimulus (n=5), a significantly larger rise in cytosolic Ca^{2+} of ~ 475%

Fig 11

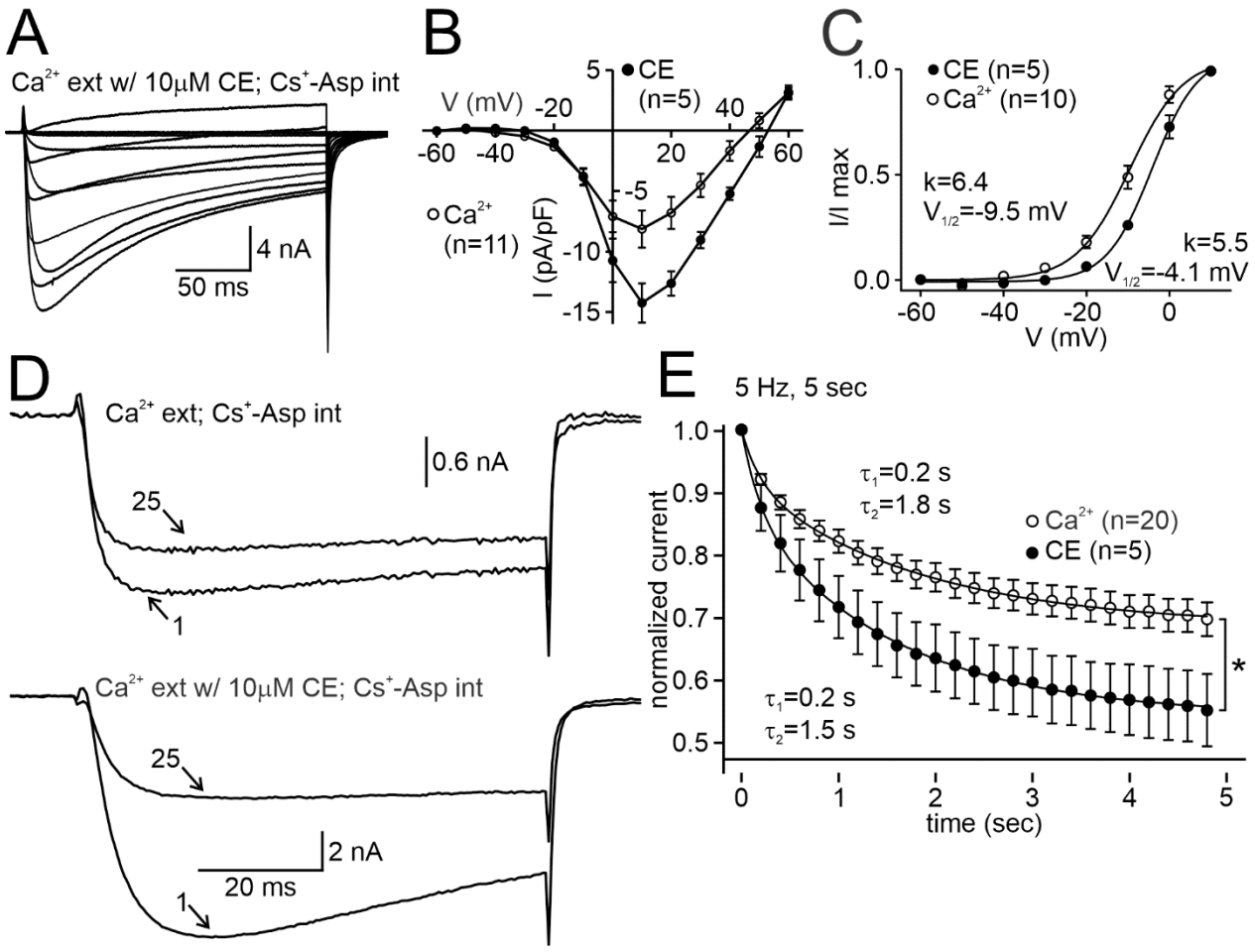

Figure 11. Inhibition of the plasma membrane Ca^{2+}-ATPase increases the extent of current rundown.

A, Whole-cell voltage-clamp recordings of Ca^{2+} current, with 10 μM carboxyeosin (CE) in the intracellular solution, evoked by 200-ms pulses from -60 mV to +60 mV in 10-mV increments. ***B,*** The mean I-V relationship of peak Ca^{2+} current density in the presence of 10 μM CE is plotted with peak control Ca^{2+} current density (reproduced from figure 4) ***C,*** Activation curve constructed by normalizing to maximum current (at +10 mV) and plotting with test voltage. The curves represent a fit with a Boltzmann function and provides a $V_{0.5}$ and k of -4.1 mV and 5.5, respectively for the CE condition, which is right-shifted compared to control (reproduced from figure 4). ***D,*** Current evoked from -80 mV with 75-ms pulses to 0 mV at 5 Hz for 5 sec. First and last sweeps are overlaid and labeled. Abscissa applies to both sets of traces. ***E,*** The mean current rundown during the train-stimulus for CE and control condition. Current is normalized to the first sweep, and curves are fit with a bi-exponential function. A comparison of the current evoked by the final step reveals that the current runs down significantly more in the CE condition (t_{23}=2.386; p=0.0257; unpaired Student's t-test).

Fig 12

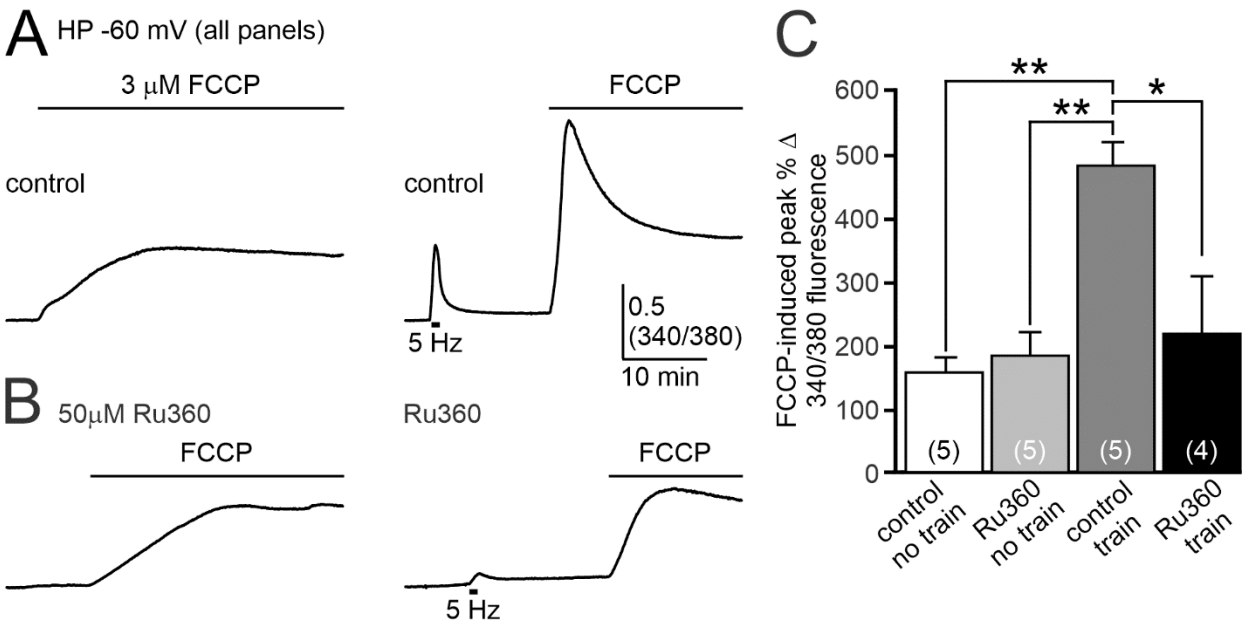

Figure 12. Voltage-gated Ca^{2+} influx loads mitochondrial Ca^{2+} stores in an Ru360-sensitive manner.

A, In control conditions, *left,* 3 μM FCCP induces a large intracellular Ca^{2+} rise in fura-filled neurons under voltage clamp at -60 mV. *Right,* A 5-Hz, 1-min train-stimulus increases the FCCP-induced intracellular Ca^{2+} rise. ***B,*** With 50 μM Ru360 in the intracellular saline, *left*, 3 μM FCCP causes a Ca^{2+} change similar to control. *Right,* A 5-Hz, 1-min train-stimulus with Ru360 does not alter the FCCP-induced Ca^{2+} rise compared to conditions. ***C,*** Summary data presenting the mean percent change in peak 340/380 fluorescence following introduction of FCCP. In the absence of prior stimulation, the FCCP-induced Ca^{2+} rise is not altered by Ru360; however, the response is significantly larger when preceded by the train-stimulus, and this augmentation is eliminated by Ru360 ($F_{3,18}$=9.912, p=0.0008, ordinary one-way ANOVA; *p<0.05, **p<0.01, Tukey-Kramer multiple comparisons test).

was observed (**Fig. 12 A, *right***). In the presence of 50 μM Ru360 with no train-stimulus applied (n=5), a similar increase in cytosolic Ca^{2+} of ~175% occurred compared to control (**Fig. 12 B, *left***). Conversely, when neurons underwent a train-stimulus prior to FCCP treatment in the presence of Ru360 (n=4), the resultant increase in cytosolic Ca^{2+} was essentially equivalent to that of the no-train Ru360 condition (**Fig. 12 B, *right***). By comparing the summary data, it was evident that following a 5-Hz, 1-min train-stimulus, Ru360 caused a significant reduction in the increase of cytosolic Ca^{2+}, when compared to control (**Fig. 12 C**). This advances the notion that the mitochondria act as a sink for voltage-gated Ca^{2+} influx, playing a key role in intracellular Ca^{2+} handling.

Chapter 4 - Discussion

Electrical activity in the nervous system is dependent on varying gradients of ions, namely, Na^+, K^+, Ca^{2+}, and Cl^-. Of these, Ca^{2+} is particularly critical thanks to its role in cell signaling in many processes, such as neuronal excitability and secretion (Clapham 2007; Giorgi et al. 2018). To affect these physiological processes, Ca^{2+} channels harness the ionic gradient and act as transducers of changes in the membrane potential to trigger second order signaling within the cell (Catterall 2011; Tsien et al. 1988; Yang and Berggren 2006). In bag cell neurons, Ca^{2+} channels mediate part of the upstroke of the action potential (Acosta-Urquidi and Dudek 1981) which produces Ca^{2+} influx necessary for Ca^{2+}-induced Ca^{2+} release (CICR) (Fisher et al. 1994; Geiger and Magoski 2008; Groten et al. 2013), secretion (Groten and Magoski 2015; Hickey et al. 2013), and channel activation (Hung and Magoski 2007; Kaczmarek and Strumwasser 1984; Lupinsky and Magoski 2006) or inactivation (Dargaei et al. 2015).

Use-dependent rundown was documented in the voltage-gated Ca^{2+} current by Hung and Magoski (2007) and Groten et al. (2013), but no mechanistic explanation was provided. I now show that rundown of the Ca^{2+} current is not only use-dependent, but that the current also undergoes Ca^{2+}-dependent inactivation (CDI) in which the entering free Ca^{2+} interacts directly with the channel to slow further influx. Furthermore, it is demonstrated that the mitochondria act as a Ca^{2+} sink during normal Ca^{2+} influx, to modulate CDI and thus play an integral role in intracellular Ca^{2+} handling.

The bag cell neuron voltage-gated Ca^{2+} current

Bag cell neurons express two distinct Ca^{2+} channel subtypes, which differ in their molecular structure of the α_1 subunit (White and Kaczmarek 1997). The research in this thesis is exclusively with the basal Ca^{2+} channel, Apl-Ca_V1 (aka BCCa-II), as opposed to the Apl-Ca_V2 (aka BCCa-I). The latter is recruited to the membrane by PKC, whereas Apl-Ca_V1 is not (Zhang

et al. 2008). The PKC-insensitive Apl-Ca_v1 channel is uniformly distributed throughout the membranes of bag cell neurons and are most similar to the vertebrate L-type channels ($Ca_v1.x$), given that they are broadly expressed in neurons, glia, and muscle (Strong et al. 1987; White and Kaczmarek 1997). Endogenous Apl-Ca_v1 is relatively slow to inactivate at depolarized voltages (Deriemer et al. 1985), partially blocked by micromolar levels of nifedipine (Nerbonne and Gurney 1987), and fully blocked by millimolar quantities of Ni^{2+}, Co^{2+}, Zn^{+}, or verapamil (Hung and Magoski 2007; Lee et al. 2023).

The ultimate goal of the influx of Ca^{2+} in bag cell neurons is to elicit egg laying hormone secretion (Fisher et al. 1994; Kaczmarek et al. 1982; Woolum and Strumwasser 1988). Here, I've demonstrated that the Ca^{2+} current has a mid-activation voltage ($V_{1/2}$) below 0 mV. This fact, combined with the relatively steep slope factor of voltage dependence means that even a moderate depolarization results in Ca^{2+} influx over much of the duration of the action potential. Similarly, when considering the somewhat slow action potential, with a half width of ~20 ms (Hung and Magoski 2007), these two factors likely contribute to the high Ca^{2+} elevation needed to trigger secretion.

The classical U-shaped current-voltage (I-V) curve observed here confirms that recordings are of a *bona fide* Ca^{2+} conductance. Isolation of this conductance was possible by substituting Cs^{+} for K^{+} in both the internal and external solutions and replacing TEA for Na^{+} externally. Originally, in the squid giant axon, Bezanilla and Armstrong (1972) showed that intracellular Cs^{+} blocks the K^{+} current. Later, Cs^{+} was successfully used to block K^{+} current so to isolate both Ca^{2+} and Na^{+} currents in *Aplysia* neurons (Colmers et al. 1982; Dargaei et al. 2014; Tillotson 1979). The I/V curve shows a strong inward current from -40 mV to +10 mV due to additional channels opening with each step. From ~ +20 mV and more positive, the current becomes progressively smaller as Cs^{+} outcompetes Ca^{2+} for channel occupancy and leaves the

neuron as outward current. For this reason, the reversal potential of the current is more negative than the theoretical equilibrium potential of ~ +250 mV for Ca^{2+} (Hille 2001).

Use-dependent rundown of the bag cell neuron voltage-gated Ca^{2+} current is largely due to Ca^{2+}-dependent inactivation

The present experiments show that Ca^{2+} current rundown is frequency dependent, with rundown increasing both with a higher frequency and longer duration train-stimulus (5-Hz vs 1-Hz, over 5 sec, ~70% vs 95% remaining; over 1 min, ~55% vs 85% remaining), strongly suggesting that a larger Ca^{2+} influx results in more current rundown. This is corroborated by Dargaei et al. (2015) who showed that the Ca^{2+} rise in bag cell neurons to a 5-Hz, 1-min stimulus train is ~ 3-fold greater than to a 1-Hz stimulus of the same duration. The available literature also presents similar evidence for frequency dependence (Groten et al. 2013; Groten and Magoski 2015; Hickey et al. 2013) and the magnitude of current rundown (Gardam et al. 2008; Hung and Magoski 2007). Here, the majority of the total rundown occurred within the first 5 sec of a given stimulus train, and as such, the 5-sec datasets were used throughout. Similarly, the 5-Hz stimulus train provided a more comprehensive representation of current rundown compared to 1-Hz.

Further evidence that use-dependence of the Ca^{2+} current is due to Ca^{2+}, and not simply cumulative inactivation, is that using external Ba^{2+} as the charger carrier prevents much of the rundown seen in control, with ~90% of the current remaining after a 5-Hz, 5-sec train-stimulus compared to 70% remaining in a Ca^{2+}-based saline. Brehm and Eckert (1978) were the first to investigate CDI, in *Paramecium*, and demonstrate that Ba^{2+}-based saline resulted in far less current rundown. This fact was later confirmed in *Aplysia* neurons (Eckert and Tillotson 1981; Tillotson 1979), and is now considered an electrophysiological hallmark, including in mammalian neurons (Budde et al. 2002). It is well established that Ba^{2+} permeates Ca^{2+} channels as well as, or better than, Ca^{2+} (Hagiwara et al. 1974; Tam et al. 2009; Yue and Marban 1990);

however, Ba^{2+} does not inactivate the channel due to its poor affinity for Ca^{2+} effector proteins, such as calmodulin (CaM) (Branchaw et al. 1997; Veselovskii and Fedulova 1986). The left-shift of the activation curve observed in the Ba^{2+}-based saline is supported by previous findings from our lab (Tam et al. 2009), and is likely due to a lesser ability of the divalent charge of Ba^{2+} to impact the voltage sensor of the channel as compared to Ca^{2+}. The exact mechanism for this however, remains undetermined (Byerly et al. 1985).

Consistent with the notion that free Ca^{2+} is a requisite for CDI, much of the rundown is prevented by the Ca^{2+} buffer, ethyleneglycol bis (aminoethylether) tetraacetic acid (EGTA). Originally implemented in *Helix* and *Lymnaea* neurons (Kostyuk and Krishtal 1977) and subsequently in *Aplysia* (Eckert and Tillotson 1981; Tillotson 1979), EGTA is now a standard means to reduce inactivation by adding an exogenous buffer (Budde et al. 2002). Although EGTA has a relatively higher affinity for Ca^{2+} (~200 nM Kd) than ATP or other endogenous intracellular buffers (μM-mM Kd), it chelates at a much slower rate (μM/sec range) than other buffers (tens of nM/sec) (Naraghi and Neher 1997). If Ca^{2+} is feeding back directly, by binding to the channel or an associated protein, or indirectly by binding a more distant effector protein, high affinity EGTA effectively outcompetes for Ca^{2+} in that environment. My findings are consistent with other Ca^{2+}-based messenger systems, which find that EGTA reduces the efficacy of Ca^{2+} as a messenger. For example, again in bag cell neurons, adding or increasing EGTA reduced the frequency of Ca^{2+}-CaM Kinase-activated cation channel opening (Hickey et al. 2010; Hung and Magoski 2007), Ca^{2+}-influx-induced secretion, presumably via SNARES (Hickey et al. 2013), and Ca^{2+}-influx-CaM Kinase inhibition of gap junctions (Dargaei et al. 2015).

Possible mechanism for CDI

Protein phosphatases and protein kinases are a primary means for inactivation of plasma membrane bound ion channels. In the case of the voltage-gated Ca^{2+} channel, phosphatases, and in particular the CaM-dependent phosphatase, calcineurin, are thought to limit Ca^{2+} influx in a Ca^{2+}-dependent manner (Armstrong 1989; Chad and Eckert 1986; Li et al. 2005). In addition to enzyme action, the predominant mechanistic hypothesis for CDI is CaM-dependent (Hell et al. 1993; Peterson et al. 1999; Zühlke et al. 1999): CaM is tethered to the IQ motif on the C-terminal tail of the Ca^{2+} channel pore-forming α subunit. When bound to Ca^{2+}, the Ca^{2+}-CaM complex closes the pore, thus inactivating the channel (Ben-Johny and Yue 2014; Budde et al. 2002; Liu and Vogel 2012; Van Petegem et al. 2005; Zühlke et al. 1999; Zühlke and Reuter 1998). The hypothesis is further bolstered by the fact that free CaM will form close and/or physical interactions with L-type Ca^{2+} channels, in order to allow for a rapid and concerted response to a spike in free intracellular Ca^{2+} (Catterall 2011).

The present study shows that bag cell neuron CDI is at least dependent on a rise in intracellular Ca^{2+}, as evidenced by the EGTA experimental data. In addition, the results of the extracellular Ba^{2+} condition are consistent with CDI being CaM dependent, in so much that, unlike Ca^{2+}, Ba^{2+} fails to activate CaM (Chao et al. 1984). For example, a direct assay of a small-conductance Ca^{2+}-activated K^+ channel shows that intracellular Ba^{2+} does not gate like Ca^{2+}, because it fails to properly bind/activate the CaM associated with the channel (Cao and Houamed 1999; Xia et al. 1998). Thus, the decrease in rundown observed with Ba^{2+} as the charge carrier could be attributed to the non-participation of CaM.

As mentioned previously, the bag cell neuron channel in question is the basal Apl-Ca_V1/BCCa-II, which has a very similar IQ motif to that of the human $Ca_V1.2$ channel used by Zuhlke et al. (1999) and Van Petegam et al. (2005) to demonstrate how CaM binds to the Ca^{2+}

channel. Seemingly all IQ residues interact with CaM, while specific aromatic residues act as anchors to presumably keep CaM in position at all times. The fact that the *Aplysia* and human channels share 82% homology in the core of the IQ motif, and 100% homology in the aromatic anchors, supports the hypothesis that CDI in bag cell neurons is CaM-dependent (White and Kaczmarek 1997). Analogously, *Aplysia* CaM differs from its human counterpart by only 3 out of 149 residues (*ie*, 98% similarity).

Mitochondrial Ca^{2+} handling as a regulator of CDI

The mitochondria are known to take up voltage-gated Ca^{2+} influx in a number of neuronal species, such as dorsal root ganglion (DRG) (Werth and Thayer 1994), sympathetic (Peng 1998), crayfish motor (Tang and Zucker 1997), higher-order sensory (calyx of Held) (Billups and Forsythe 2002), and hippocampal neurons (Chamberland et al. 2019; Katsenelson et al. 2022; Marland et al. 2016), as well as several neuroendocrine cells including, chromaffin cells (Herrington et al. 1996) and gonadotropes (Kaftan et al. 2000). Thus, understanding the basis of the mitochondrial role in CDI has general implications for neuronal function.

Previous work from our laboratory (Groten et al. 2013, 2016) indicates that, based on the rate of recovery following a 1-min train-stimulus, bag cell neuron voltage-gated Ca^{2+} influx is handled by two principal transport proteins. The dominant factor is the mitochondrial Ca^{2+} uniporter (MCU), which is sensitive to Ru360, while there is a lesser contribution from the plasma membrane Ca^{2+}-ATPase (PMCA), which is sensitive to La^{3+} and carboxyeosin (CE). The remaining free Ca^{2+} is presumably buffered by other cytoplasmic components, which are currently undefined. Uncertainty of these components notwithstanding, we have previously confirmed that the cytoplasmic buffering is not sensitive to the sarcoendoplasmic reticulum Ca^{2+}-ATPase (SERCA) blocker, cyclopiazonic acid (CPA), high-levels of extracellular Na^{+} to prevent Na^{+}/Ca^{2+} exchange, or bafilomycin, which halts Ca^{2+} uptake by acidic stores (Groten et al. 2013,

2016). Accordingly, Groten et al. (2013) showed Ca^{2+} influx following a train-stimulus loads into the mitochondria, as evidenced by an increase in the carbonyl cyanide 4-(trifluoromethoxy) phenylhydrazone (FCCP)-induced Ca^{2+} response. This finding is confirmed here (**Fig. 12 A**), where the FCCP-induced Ca^{2+} liberation was increased following a train, and subsequently prevented by including Ru360 in the pipette. Parenthetically, I find that blocking the MCU does not impact basal mitochondrial Ca^{2+}, suggesting the reagent is acting by preventing uptake rather than altering metabolism or steady-state Ca^{2+} release.

Under the appropriate conditions, following a 1-min train-stimulus with no intracellular EGTA, the Ca^{2+} taken up by the mitochondria is released back into the cytosol (via CICR) and then pumped out of the cell by the Na^{+}/Ca^{2+} exchanger and the PMCA (Groten et al. 2013). That stated, it is unlikely that this phenomenon plays a role in the CDI observed here over the 5-sec or 1-min train-stimulus, as mitochondrial CICR has been shown to develop only ~1 min after the 1-min train-stimulus and does not occur at all following a 5-sec train-stimulus (Groten et al. 2013, 2016).

Given figure 5, which shows that collapse of the mitochondrial membrane potential with FCCP results in greater Ca^{2+} current rundown over a 1-min train-stimulus, and the data presented in figure 10, which shows that inhibiting the MCU with Ru360 results in greater rundown over 5 sec, it appears that CDI is governed, at least in part, by mitochondrial uptake of Ca^{2+}. Paradoxically, as shown in figure 6, when the mitochondrial sink is removed with either FCCP or Ru360, the Ca^{2+} elevation evoked by a 1-min train-stimulus is reduced by about half. At first glance, one might expect a larger Ca^{2+} elevation, given that the entering Ca^{2+} has nowhere to go, but the buildup of cytosolic Ca^{2+} must be large and fast enough to quickly inactivate the channel, such that CDI curbs Ca^{2+} influx much faster than when the mitochondrial sink is in play.

While mitochondrial Ca^{2+} handling has been demonstrated to play a role neuronal processes like firing rate (Katsenelson et al. 2022), synaptic transmission (Billups and Forsythe 2002), post-tentanic potentiation (Tang and Zucker 1997), and endocytosis (Marland et al. 2016), there are few examples indicating an impacting on CDI, save for in cardiomyocytes (Sánchez et al. 2001), cerebellar granule (Budd and Nicholls 1996), chromaffin (Hernández-Guijo et al. 2001), and amarcrine (Sánchez et al. 2001) cells.

Ca^{2+} handling by the PMCA as a regulator of CDI

Although often given less attention in the literature, the PMCA also handles voltage-gated Ca^{2+} influx in the DRG, to regulate afterhyperpolarization and excitability (Ghosh et al. 2011; Usachev et al. 2002), Purkinje neurons, to influence hindlimb coordination (Empson et al. 2010), hippocampal neurons, which controls miniature EPSP amplitude and paired pulse facilitation (Jensen et al. 2007), as well as in retinal neurons (Krizaj and Copenhagen 1998; Zenisek and Matthews 2000). In bag cell neurons, the CE experiments from the present work appear to be a rare, if not the only, report of the PMCA influencing CDI. Given that the mitochondria, compared to the PMCA, have a much greater role in Ca^{2+} clearance in bag cell neurons, it is enigmatic as to why the two mechanisms appear to have nearly the same impact on CDI. Remarkably, blocking the PMCA increases loading of the mitochondria by a train-stimulus (Groten et al. 2016); as such, one might expect less CDI in the presence of CE. A simple explanation may be a matter of proximity: presumably, the PMCA is closer to the channel (as they are both plasma membrane-bound) than the mitochondria, so despite the PMCA being a less effective clearance mechanism, it can have a similar impact on CDI in the short term ($\leq$ 5-sec).

In an attempt to clarify these paradoxical findings, I performed the seemingly obvious experiment of exposing the cells to CE and Ru360 simultaneously, but it consistently killed the neurons. CE in general appeared to be somewhat toxic to the cells, either directly through its

action on the PMCA or perhaps due to an off-target effect. The alternative PMCA blocker, La^{3+}, was not feasible because at the effective concentration, it would block the Ca^{2+} current. Similarly, I also tried to short-circuit the PMCA with a high-pH external saline, but that again had an off-target effect on the Ca^{2+} current, in that it actually decreased CDI and altered the current-voltage relationship.

Possible physiological impact and future directions

By studying the dynamics of intracellular Ca^{2+} handling, and their impacts on CDI, I am able to draw several conclusions that may have implications for bag cell neuron function and neuroendocrine cells in general. The mitochondria and PMCA regulate the extent of Ca^{2+} influx through the Apl-Ca_V1 voltage-gated Ca^{2+} channel. Without their involvement, CDI would dominate Ca^{2+} channel function, resulting in less overall Ca^{2+} influx and potentially reduced excitability, suppressed Ca^{2+}-dependent gating of other channels, and importantly, less secretion.

To further elucidate the role and impact of CDI, future experiments might investigate the role for CDI in use-dependent changes in other key neuronal functions such as secretion. As secretion is known to be very sensitive to the extent of Ca^{2+} influx (Hickey et al. 2013), it stands to reason that manipulation of the rundown may result in impactful changes to the degree of peptide secretion. In this scenario, one could monitor the cellular capacitance under whole-cell voltage-clamp; any increase in membrane capacitance would indicate a proportional increase in membrane area, and thus, secretion. Other continuations of this work should be done to examine the effect of CDI on electrical coupling of bag cell neurons. As the bag cell gap junctions have been shown to be inhibited in a CaM kinase-sensitive manner (Dargaei et al., 2015), I would expect to see less Ca^{2+}-dependent inhibition of junctional conductance when run-down is increased by Ru360 or other means. This would have implications for how electrical coupling is

regulated during the continuous firing (and Ca^{2+} influx) of the afterdischarge, and electrically coupled systems as a whole.

References

Acosta-Urquidi J, **Dudek FE**. Soma spike of neuroendocrine bag cells of *Aplysia californica*. *J Neurobiol* 12: 367–378, 1981.

Ahlijanian MK, **Westenbroek RE**, **Catterall WA**. Subunit structure and localization of dihydropyridine-sensitive calcium channels in mammalian brain, spinal cord, and retina. *Neuron* 4: 819–832, 1990.

Akaike N, **Tsuda Y**, **Oyama Y**. Separation of current- and voltage-dependent inactivation of calcium current in frog sensory neuron. *Neurosci Lett* 84: 46–50, 1988.

Al-Jobore A, **Roufogalis BD**. Influence of EGTA on the apparent Ca^{2+} affinity of Mg^{2+}-dependent, Ca^{2+}-stimulated ATPase in the human erythrocyte membrane. *BBA - Biomembranes* 645: 1–9, 1981.

Ames JB. L-type Ca^{2+} channel regulation by calmodulin and CaBP1. *Biomolecules* 11, 2021.

Arch S. Biosynthesis of the egg-laying hormone (ELH) in the bag cell neurons of *Aplysia californica*. *Journal of General Physiology* 60: 102–119, 1972.

Arikkath J, **Campbell KP**. Auxiliary subunits: essential components of the voltage-gated calcium channel complex. *Curr Opin Neurobiol* 13: 298–307, 2003.

Armstrong DL. Calcium channel regulation by calcineurin, a Ca^{2+}-activated phosphatase in mammalian brain. *Trends Neurosci* 12: 117–122, 1989.

Baker PF, **Hodgkin AL**, **Ridgway EB**. Depolarization and calcium entry in squid giant axons. *J Physiol* 218: 709–755, 1971.

Bartel DP, **Sheng M**, **Lau LF**, **Greenberg ME**. Growth factors and membrane depolarization activate distinct programs of early response gene expression: dissociation of fos and jun induction. *Genes Dev* 3: 304–313, 1989.

Ben-Johny M, **Yue DT**. Calmodulin regulation (calmodulation) of voltage-gated calcium channels. *J Gen Physiol*: 679–692, 2014.

Bennett MK. Ca^{2+} and the regulation of neurotransmitter secretion. *Curr Opin Neurobiol* 7: 316–322, 1997.

Berridge MJ. Neuronal calcium signaling. *Neuron* 21: 13–26, 1998.

Bers DM. Cardiac excitation-contraction coupling. *Nature* 415: 198–205, 2002.

Bezanilla F, **Armstrong CM**. Negative conductance caused by entry of sodium and cesium ions into the potassium channels of squid axons. *J Gen Physiol* 60: 588–608, 1972.

Bicknell RJ. Optimizing release from peptide hormone secretory nerve terminals. *Exp Biol* 139: 51–65, 1988.

Bicknell RJ, **Leng G**. Relative efficiency of neural firing patterns for vasopressin release *in vitro*. *Neuroendocrinology* 33: 295–299, 1981.

Billups B, **Forsythe ID**. Presynaptic mitochondrial calcium sequestration influences transmission at mammalian central synapses. *J Neurosci* 22: 5840–5847, 2002.

Bollimuntha S, **Pani B**, **Singh BB**. Neuronal store-operated Ca^{2+} signaling: An overview and its function. *Adv Exp Med Biol* 993: 535, 2017.

Branchaw JL, **Banks MI**, **Jackson MB**. Ca^{2+} - and voltage-dependent inactivation of Ca^{2+} channels in nerve terminals of the neurohypophysis. *Neurosci* 17: 5772–5781, 1997.

Brehm P, **Eckert R**. Calcium entry leads to inactivation of calcium channel in Paramecium. *Science (1979)* 202: 1203–1206, 1978.

Brini M, **Calì T**, **Ottolini D**, **Carafoli E**. Neuronal calcium signaling: function and dysfunction Introduction: general principle of Ca^{2+} signaling. *Cell Mol Life Sci* 71: 2787–2814, 2014.

Brownstein MJ, **Russell JT**, **Gainer H**. Synthesis, transport, and release of posterior pituitary hormones. *Science* 207: 373–378, 1980.

Budd SL, **Nicholls DG**. A reevaluation of the role of mitochondria in neuronal Ca^{2+} homeostasis. *J Neurochem* 66: 403–411, 1996.

Budde T, **Meuth S**, **Pape HC**. Calcium-dependent inactivation of neuronal calcium channels. *Nat Rev Neurosci* 3: 873–883, 2002.

Byerly L, **Bryant Chase P**, **Stimers JR**. Permeation and interaction of divalent cations in calcium channels of snail neurons. *J Gen Physiol* 85: 491–518, 1985.

Cao YJ, **Houamed KM**. Activation of recombinant human SK4 channels by metal cations. *FEBS Lett* 446: 137–141, 1999.

Capiod T, **Mauger J-P**, **Binet A**, **Claret M**. *Regulation of calcium in non-excitable cells*. 1989.

Catterall WA. Voltage-gated calcium channels. *Cold Spring Harb Perspect Biol* 3: 1–23, 2011.

Cens T, **Rousset M**, **Leyris JP**, **Fesquet P**, **Charnet P**. Voltage- and calcium-dependent inactivation in high voltage-gated Ca^{2+} channels. *Prog Biophys Mol Biol* 90: 104–117, 2006.

Chad JE, **Eckert R**. An enzymatic mechanism for calcium current inactivation in dialysed *Helix* neurones. *J Physiol* 378: 31–51, 1986.

Chamberland S, **Zamora Moratalla A**, **Topolnik L**. Calcium extrusion mechanisms in dendrites of mouse hippocampal CA1 inhibitory interneurons. *Cell Calcium* 77: 49–57, 2019.

Chang FC, **Hoseys MM**. Dihydropyridine and phenylalkylamine receptors associated with cardiac and skeletal muscle calcium channels are structurally different. *J Biol Chem* 263: 18929–18937, 1988.

Chao SH, **Suzuki Y**, **Zysk JR**, **Cheung WY**. Activation of calmodulin by various metal cations as a function of ionic radius. *Mol Pharmacol* 26, 1984.

Chapman ER. Synaptotagmin: A Ca^{2+} sensor that triggers exocytosis? *Nat Rev Mol Cell Biol* 3: 498–508, 2002.

Chiu AY, **Hunkapiller MW**, **Heller E**, **Stuart DK**, **Hood LE**, **Strumwasser F**. Purification and primary structure of the neuropeptide egg-laying hormone of *Aplysia californica*. *Proc Natl Acad Sci U S A* 76: 6656–6660, 1979.

Clapham DE. Calcium signaling. *Cell* 131: 1047–1058, 2007.

Colmers WF, **Lewis D V.**, **Wilson WA**. Cs^{+} loading reveals Na^{+}-dependent persistent inward current and negative slope resistance region in *Aplysia* giant neurons. *J Neurophysiol* 48: 1191–1200, 1982.

Coussens L, **Parker PJ**, **Rhee L**, **Yang-Feng TL**, **Chen E**, **Waterfield MD**, **Francke U**, **Ullrich A**. Multiple, distinct forms of bovine and human protein kinase C suggest diversity in cellular signaling pathways. *Science (1979)* 233: 859–866, 1986.

Dargaei Z, **Colmers PLW**, **Hodgson HM**, **Magoski NS**. Electrical coupling between *Aplysia* bag cell neurons: characterization and role in synchronous firing. *J Neurophysiol* 112: 2680–2696, 2014.

Dargaei Z, **Standage D**, **Groten CJ**, **Blohm G**, **Magoski NS**. Ca^{2+}-induced uncoupling of *Aplysia* bag cell neurons. *J Neurophysiol* 113: 808–821, 2015.

Deisseroth K, **Heist EK**, **Tsien RW**. Translocation of calmodulin to the nucleus supports CREB phosphorylation in hippocampal neurons. *Nature* 392: 198–202, 1998.

Deriemer SA, **Strong JA**, **Albert KA**, **Greengard P**, **Kaczmarek LK**. Enhancement of calcium current in *Aplysia* neurones by phorbol ester and protein kinase C. *Nature* 313: 313–316, 1985.

Dodge FA, **Rahamimoff R**. Co-operative action of calcium ions in transmitter release at the neuromuscular junction. *J Physiol* 193: 419–432, 1967.

Dolphin AC. Voltage-gated calcium channels and their auxiliary subunits: physiology and pathophysiology and pharmacology. *J Physiol* 594: 5369–5390, 2016.

Eckert R, **Tillotson DL**. Calcium-mediated inactivation of the calcium conductance in caesium-loaded giant neurones of *Aplysia californica*. *J Physiol* 314: 265–280, 1981.

Empson RM, **Turner PR**, **Nagaraja RY**, **Beesley PW**, **Knöpfel T**. Reduced expression of the Ca^{2+} transporter protein PMCA2 slows Ca^{2+} dynamics in mouse cerebellar Purkinje neurones and alters the precision of motor coordination. *J Physiol* 588: 907–922, 2010.

Ertel EA, **Campbell KP**, **Harpold MM**, **Hofmann F**, **Mori Y**, **Perez-Reyes E**, **Schwartz A**, **Snutch TP**, **Tanabe T**, **Birnbaumer L**, **Tsien RW**, **Catterall WA**. Nomenclature of voltage-gated calcium channels. *Neuron* 25: 533–535, 2000.

Fernández-Chacón R, **Königstorfer A**, **Gerber SH**, **García J**, **Matos MF**, **Stevens CF**, **Brose N**, **Rizo J**, **Rosenmund C**, **Südhof TC**. Synaptotagmin I functions as a calcium regulator of release probability. *Nature* 410: 41–49, 2001.

Fisher TE, **Levy S**, **Kaczmarek LK**. Transient changes in intracellular calcium associated with a prolonged increase in excitability in neurons of *Aplysia californica*. *J Neurophysiol* 71: 1254–1257, 1994.

Frazier WT, **Kandel ER**, **Kupfermann I**, **Waziri R**, **Coggeshall RE**. Morphological and functional properties of identified neurons in the abdominal ganglion of *Aplysia californica*. *J Neurophysiol* 30: 1288–1351, 1967.

Gardam KE, **Geiger JE**, **Hickey CM**, **Hung AY**, **Magoski NS**. Flufenamic acid affects multiple currents and causes intracellular Ca^{2+} release in *Aplysia* bag cell neurons. *J Neurophysiol* 100: 38–49, 2008.

Gatto C, **Milanick MA**. Inhibition of the red blood cell calcium pump by eosin and other fluorescein analogues. *Am J Physiol Cell Physiol* 264, 1993.

Geiger JE, **Magoski NS**. Ca^{2+}-induced Ca^{2+} release in *Aplysia* bag cell neurons requires interaction between mitochondrial and endoplasmic reticulum stores. *J Neurophysiol* 100: 24–37, 2008.

Ghosh A, **Greenberg ME**. Calcium signaling in neurons: Molecular mechanisms and cellular consequences. *Science (1979)* 268: 239–247, 1995.

Ghosh B, **Li Y**, **Thayer SA**. Inhibition of the plasma membrane Ca^{2+} pump by CD44 receptor activation of tyrosine kinases increases the action potential afterhyperpolarization in sensory neurons. *J Neurosci* 31: 2361, 2011.

Giorgi C, **Danese A**, **Missiroli S**, **Patergnani S**, **Pinton P**. Calcium dynamics as a machine for decoding signals. *Trends Cell Biol* 28: 258–273, 2018.

Green AK, **Cobbold PH**, **Dixon CJ**. Effects on the hepatocyte [Ca^{2+}] oscillator of inhibition of the plasma membrane Ca^{2+} pump by carboxyeosin or glucagon. *Cell Calcium* 22: 99–109, 1997.

Groten CJ, **Magoski NS**. PKC enhances the capacity for secretion by rapidly recruiting covert voltage-gated Ca^{2+} channels to the membrane. *Journal of Neuroscience* 35: 2747–2765, 2015.

Groten CJ, **Rebane JT**, **Blohm G**, **Magoski NS**. Separate Ca^{2+} sources are buffered by distinct Ca^{2+} handling systems in *Aplysia* neuroendocrine cells. *J Neurosci* 33: 6476–6491, 2013.

Groten CJ, **Rebane JT**, **Hodgson HM**, **Chauhan AK**, **Blohm G**, **Magoski NS**. Ca^{2+} removal by the plasma membrane ca^{2+}-atpase influences the contribution of mitochondria to activity-dependent Ca^{2+} dynamics in *Aplysia* neuroendocrine cells. *J Neurophysiol* 115: 2615–2634, 2016.

Guerini D. Calcineurin: Not just a simple protein phosphatase. *Biochem Biophys Res Commun* 235: 271–275, 1997.

Van Haasteren G, **Li S**, **Muda M**, **Susini S**, **Schlegel W**. Calcium signalling and gene expression. In: *J Rec Sig Transduct Res*, 1999, p. 481–492.

Hagiwara S, **Fukuda J**, **Eaton DC**. Membrane currents carried by Ca, Sr, and Ba in barnacle muscle fiber during voltage clamp. *J Gen Physiol* 63: 564–578, 1974.

Hell JW, **Yokoyama CT**, **Wong ST**, **Warner C**, **Snutch TP**, **Catterall WA**. Differential phosphorylation of two size forms of the neuronal class C L-type calcium channel alpha 1 subunit. *J Biol Chem* 268: 19451–7, 1993.

Hernández-Guijo JM, **Maneu-Flores VE**, **Ruiz-Nuño A**, **Villarroya M**, **García AG**, **Gandía L**. Calcium-dependent inhibition of L, N, and P/Q Ca^{2+} channels in chromaffin cells: role of mitochondria. *J Neurosci* 21: 2553–2560, 2001.

Herrington J, **Park YB**, **Babcock DF**, **Hille B**. Dominant role of mitochondria in clearance of large Ca^{2+} loads from rat adrenal chromaffin cells. *Neuron* 16: 219–228, 1996.

Heytler PG, **Prichard WW**. A new class of uncoupling agents--carbonyl cyanide phenylhydrazones. *Biochem Biophys Res Commun* 7: 272–275, 1962.

Hickey CM, **Geiger JE**, **Groten CJ**, **Magoski NS**. Mitochondrial Ca^{2+} activates a cation current in *Aplysia* bag cell neurons. *J Neurophysiol* 103: 1543–1556, 2010.

Hickey CM, **Groten CJ**, **Sham L**, **Carter CJ**, **Magoski NS**. Voltage-gated Ca^{2+} influx and mitochondrial Ca^{2+} initiate secretion from *Aplysia* neuroendocrine cells. *Neuroscience* 250: 755–772, 2013.

Hille B. Ionic channels of Excitable Membranes 2nd edition [Online]. Third Edition. Sinauer Associates.https://global.oup.com/academic/product/ion-channels-of-excitable-membranes-9780878933211, 2001.

Hung AY, **Magoski NS**. Activity-dependent initiation of a prolonged depolarization in *Aplysia* bag cell neurons: role for a cation channel. *J Neurophysiol* 97: 2465–2479, 2007.

Jahn R, **Scheller RH**. SNAREs - Engines for membrane fusion. *Nat Rev Mol Cell Biol* 7: 631–643, 2006.

Jensen TP, **Filoteo AG**, **Knopfel T**, **Empson RM**. Presynaptic plasma membrane Ca^{2+} ATPase isoform 2a regulates excitatory synaptic transmission in rat hippocampal CA3. *J Physiol* 579: 85–99, 2007.

Johnson CM, **Hill CS**, **Chawla S**, **Treisman R**, **Bading H**. Calcium controls gene expression via three distinct pathways that can function independently of the Ras/mitogen-activated protein kinases (ERKs) signaling cascade. *J Neurosci* 17: 6189–6202, 1997.

Kaczmarek LK, **Finbow M**, **Revel JP**, **Strumwasser F**. The morphology and coupling of Aplysia bag cells within the abdominal ganglion and in cell culture. *J Neurobiol* 10: 535–550, 1979.

Kaczmarek LK, **Jennings KR**, **Strumwasser F**. An early sodium and a late calcium phase in the afterdischarge of peptide-secreting neurons of *Aplysia*. *Brain Res* 238: 105–115, 1982.

Kaczmarek LK, **Strumwasser F**. A voltage-clamp analysis of currents underlying cyclic AMP-induced membrane modulation in isolated peptidergic neurons of *Aplysia*. *J Neurophysiol* 52: 340–349, 1984.

Kaftan EJ, **Xu T**, **Abercrombie RF**, **Hille B**. Mitochondria shape hormonally induced cytoplasmic calcium oscillations and modulate exocytosis. *J Biol Chem* 275: 25465–25470, 2000.

Katsenelson M, **Shapira I**, **Abbas E**, **Jevdokimenko K**, **Styr B**, **Ruggiero A**, **Aïd S**, **Fornasiero EF**, **Holzenberger M**, **Rizzoli SO**, **Slutsky I**. IGF-1 receptor regulates upward firing rate homeostasis via the mitochondrial calcium uniporter. *Proc Natl Acad Sci U S A* 119, 2022.

Katz B, **Miledi R**. Ionic requirements of synaptic transmitter release. *Nature*: 651, 1967.

Kits KS, **Mansvelder HD**. Voltage gated calcium channels in molluscs: classification, Ca^{2+} dependent inactivation, modulation and functional roles. *Invert Neurosci* 2: 9–34, 1996.

Knox RJ, **Jonas EA**, **Kao L Sen**, **Smith PJS**, **Connor JA**, **Kaczmarek LK**. Ca^{2+} influx and activation of a cation current are coupled to intracellular Ca^{2+} release in peptidergic neurons of *Aplysia californica*. *J Physiol* 494: 627–639, 1996.

Kostyuk PG, **Krishtal OA**. Effects of calcium and calcium-chelating agents on the inward and outward current in the membrane of mollusc neurones. *J Physiol* 270: 569–580, 1977.

Kramer RH, **Zucker RS**. Calcium-dependent inward current in *Aplysia* bursting pace-maker neurones. *J Physiol* 362: 107–130, 1985.

Krizaj D, **Copenhagen DR**. Compartmentalization of calcium extrusion mechanisms in the outer and inner segments of photoreceptors. *Neuron* 21: 249–256, 1998.

Kupfermann I, **Kandel ER**. Electrophysiological properties and functional interconnections of two symmetrical neurosecretory clusters (bag cells) in abdominal ganglion of *Aplysia*. *J Neurophysiol* 33: 865–876, 1970.

Lee A, **Wong ST**, **Gallagher D**, **Li B**, **Storm DR**, **Scheuer T**, **Catterall WA**. Ca^{2+}/calmodulin binds to and modulates P/Q-type calcium channels. *Nature* 399: 155–159, 1999.

Lee D, **Lee KH**, **Ho WK**, **Lee SH**. Target cell-specific involvement of presynaptic mitochondria in post-tetanic potentiation at hippocampal mossy fiber synapses. *Journal of Neuroscience* 27: 13603–13613, 2007.

Lee KH, **Wassef DE**, **MacNeil EK**, **Magoski NS**. Cholinergic depolarization recruits a persistent Ca^{2+} current in *Aplysia* bag cell neurons. *J Neurophysiol* 129: 1045–1060, 2023.

Li D, **Wang F**, **Lai M**, **Chen Y**, **Zhang JF**. A protein phosphatase 2cα-Ca^{2+} channel complex for dephosphorylation of neuronal Ca^{2+} channels phosphorylated by protein kinase C. *J Neurosci* 25: 1914, 2005.

Liman ER. Regulation by voltage and adenine nucleotides of a Ca^{2+}-activated cation channel from hamster vomeronasal sensory neurons. *J Physiol* 548: 777–787, 2003.

Lipscombe D, **Helton TD**, **Xu W**. L-type calcium channels: the low down. 2004. doi:10.1152/jn.00486.2004.

Lipscombe D, **Madison D V.**, **Poenie M**, **Reuter H**, **Tsien RW**, **Tsien RY**. Imaging of cytosolic Ca^{2+} transients arising from Ca^{2+} stores and Ca^{2+} channels in sympathetic neurons. *Neuron* 1: 355–365, 1988.

Liu Z, **Vogel HJ**. Structural basis for the regulation of L-type voltage-gated calcium channels: interactions between the N-terminal cytoplasmic domain and Ca^{2+}-calmodulin. *Front Mol Neurosci* 5: 1–46, 2012.

Lupinsky DA, **Magoski NS**. Ca^{2+}-dependent regulation of a non-selective cation channel from *Aplysia* bag cell neurones. *J Physiol* 575: 491, 2006.

Marland JRK, **Hasel P**, **Bonnycastle K**, **Cousin MA**. Mitochondrial calcium uptake modulates synaptic vesicle endocytosis in central nerve terminals. *J Biol Chem* 291: 2080–2086, 2016.

Marrion N V., **Tavalin SJ**. Selective activation of Ca^{2+}-activated K^+ channels by co-localized Ca^{2+} channels in hippocampal neurons. *Nature* 395: 900–905, 1998.

Matlib MA, **Zhou Z**, **Knight S**, **Ahmed S**, **Choi KM**, **Krause-Bauer J**, **Phillips R**, **Altschuld R**, **Katsube Y**, **Sperelakis N**, **Bers DM**. Oxygen-bridged dinuclear ruthenium amine complex specifically inhibits Ca^{2+} uptake into mitochondria in vitro and in situ in single cardiac myocytes. *J Biol Chem* 273: 10223–10231, 1998.

McManus OB. Calcium-activated potassium channels: Regulation by calcium. *J Bioenerg Biomembr* 23: 537–560, 1991.

Meinrenken CJ, **Borst JGG**, **Sakmann B**. Local routes revisited: The space and time dependence of the Ca^{2+} signal for phasic transmitter release at the rat calyx of Held. *Physiol* 547: 665–689, 2003.

Moore SJ, **Murphy GG**. The role of L-type calcium channels in neuronal excitability and aging. *Neurobiol Learn Mem* 173, 2020.

Naraghi M, **Neher E**. Linearized buffered Ca^{2+} diffusion in microdomains and its implications for calculation of $[Ca^{2+}]$ at the mouth of a calcium channel. *J Neurosci* 17: 6961–6973, 1997.

Neering IR, **McBurney RN**. Role for microsomal Ca storage in mammalian neurones? *Nature* 309: 158–160, 1984.

Nerbonne JM, **Gurney AM**. Blockade of Ca^{2+} and K^+ currents in bag cell neurons of *Aplysia* californica by dihydropyridine Ca^{2+} antagonists. *J Neurosci* 7: 882–893, 1987.

Pang ZP, **Shin OH**, **Meyer AC**, **Rosenmund C**, **Südhof TC**. A gain-of-function mutation in synaptotagmin-1 reveals a critical role of Ca^{2+}-dependent soluble N-ethylmaleimide-sensitive factor attachment protein receptor complex binding in synaptic exocytosis. *J Neurosci* 26: 12556–12565, 2006.

Peng YY. Effects of mitochondrion on calcium transients at intact presynaptic terminals depend on frequency of nerve firing. *J Neurophysiol* 80: 186–195, 1998.

Peng YY, **Horn JP**. Continuous repetitive stimuli are more effective than bursts for evoking LHRH release in bullfrog sympathetic ganglia. *J Neurosci* 11: 85–95, 1991.

Van Petegem F, **Chatelain FC**, **Minor DL**. Insights into voltage-gated calcium channel regulation from the structure of the $Ca_V1.2$ IQ domain-Ca^{2+}/calmodulin complex. *Nat Struct Mol Biol* 12: 1108–1115, 2005.

Peterson BZ, **DeMaria CD**, **Yue DT**. Calmodulin is the Ca^{2+} sensor for Ca^{2+}-dependent inactivation of L- type calcium channels. *Neuron* 22: 549–558, 1999.

Pinsker HM, **Edward Dudek F**. Bag cell control of egg laying in freely behaving *Aplysia*. *Science* 197: 490–493, 1977.

Von Poser C, **Ichtchenko K**, **Shao X**, **Rizo J**, **Südhof TC**. The evolutionary pressure to inactivate: A subclass of synaptotagmins with an amino acid substitution that abolishes Ca^{2+} binding. *J Biol Chem* 272: 14314–14319, 1997.

Purves D, **Augustine GJ**, **Fitzpatrick D**, **Katz LC**, **LaMantia A-S**, **McNamara JO**, **Williams SM**. *Neuroscience*. 2nd ed. Sunderland, Massachusetts: Sinauer Associates, 2001.

Rettig J, **Neher E**. Emerging roles of presynaptic proteins in Ca^{++}-triggered exocytosis. *Science (1979)* 298: 781–785, 2002.

Richter TA, **Kolaj M**, **Renaud LP**. Low voltage-activated Ca^{2+} channels are coupled to Ca^{2+}-induced Ca^{2+} release in rat thalamic midline neurons. *J Neurosci* 25: 8267–8271, 2005.

Robitaille R, **Garcia ML**, **Kaczorowski GJ**, **Chariton MP**. Functional colocalization of calcium and calcium-gated potassium channels in control of transmitter release. *Neuron* 11: 645–655, 1993.

Sabatini BL, **Regehr WG**. Timing of neurotransmission at fast synapses in the mammalian brain. *Nature* 384: 170–172, 1996.

Sánchez JA, **García MC**, **Sharma VK**, **Young KC**, **Matlib MA**, **Sheu SS**. Mitochondria regulate inactivation of L-type Ca^{2+} channels in rat heart. *J Physiol* 536: 387–396, 2001.

Sheng M, **McFadden G**, **Greenberg ME**. Membrane depolarization and calcium induce c-fos transcription via phosphorylation of transcription factor CREB. *Neuron* 4: 571–582, 1990.

Simms BA, **Zamponi GW**. Neuronal voltage-gated calcium channels: Structure, function, and dysfunction. *Neuron* 82: 24–45, 2014.

Spafford JD, **Dunn T**, **Smit AB**, **Syed NI**, **Zamponi GW**. *In vitro* characterization of L-type calcium channels and their contribution to firing behavior in invertebrate respiratory neurons. *J Neurophysiol* 95: 42–52, 2006.

Stanley EF. Single calcium channels and acetylcholine release at a presynaptic nerve terminal. *Neuron* 11: 1007–1011, 1993.

Stotz SC, **Zamponi GW**. Structural determinants of fast inactivation of high voltage-activated Ca^{2+} channels. *Trends Neurosci* 24: 176–182, 2001.

Strong JA, **Fox AP**, **Tsien RW**, **Kaczmarek LK**. Stimulation of protein kinase C recruits covert calcium channels in *Aplysia* bag cell neurons. *Nature* 325: 714–717, 1987.

Sturgeon RM, **Chauhan AK**, **Magoski NS**. Neuroendocrine control of reproduction in *Aplysia* by the bag cell neurons. *Model Animals in Neuroendocrinology* 29–58, 2018.

Südhof TC. Calcium control of neurotransmitter release. *Cold Spring Harb Perspect Biol* 4, 2012.

Swartz KJ, **Merritt A**, **Bean BP**, **Lovinger DM**. Protein kinase C modulates glutamate receptor inhibition of Ca^{2+} channels and synaptic transmission. *Nature* 361: 165–168, 1993.

Tam AKH, **Geiger JE**, **Hung AY**, **Groten CJ**, **Magoski NS**. Persistent Ca^{2+} current contributes to a prolonged depolarization in *Aplysia* bag cell neurons. *J Neurophysiol* 102: 3753–3765, 2009.

Tanabe T, **Mikami A**, **Niidome T**, **Numa S**, **Adams BA**, **Beam KG**. Structure and function of voltage-dependent calcium channels from muscle. *Ann N Y Acad Sci* 707: 81–86, 1993.

Tang YG, **Zucker RS**. Mitochondrial involvement in post-tetanic potentiation of synaptic transmission. *Neuron* 18: 483–491, 1997.

Thore S, **Dyachok O**, **Gylfe E**, **Tengholm A**. Feedback activation of phospholipase C via intracellular mobilization and store-operated influx of Ca^{2+} in insulin-secreting beta-cells. *J Cell Sci* 118: 4463–4471, 2005.

Tillotson D. Inactivation of Ca conductance dependent on entry of Ca ions in molluscan neurons. *Proc Natl Acad Sci U S A* 76: 1497–1500, 1979.

Tsien RW, **Lipscombe D**, **Madison D V.**, **Bley KR**, **Fox AP**. Multiple types of neuronal calcium channels and their selective modulation. *Trends Neurosci* 11: 431–438, 1988.

Usachev YM, **DeMarco SJ**, **Campbell C**, **Strehler EE**, **Thayer SA**. Bradykinin and ATP accelerate Ca^{2+} efflux from rat sensory neurons via protein kinase C and the plasma membrane Ca^{2+} pump isoform 4. *Neuron* 33: 113–122, 2002.

Veselovskii NS, **Fedulova SA**. Effects of substituting barium for calcium ions during research into inward currents in mammalian neurons. *Neurophysiology* 18: 227–231, 1986.

Vorndran C, **Minta A**, **Poenie M**. New fluorescent calcium indicators designed for cytosolic retention or measuring calcium near membranes. *Biophys J* 69: 2112–2124, 1995.

Wadel K, **Neher E**, **Sakaba T**. The coupling between synaptic vesicles and Ca^{2+} channels determines fast neurotransmitter release. *Neuron* 53: 563–575, 2007.

Wayne NL, **Lee W**, **Kim YJ**. Persistent activation of calcium-activated and calcium-independent protein kinase C in response to electrical afterdischarge from peptidergic neurons of *Aplysia*. *Brain Res* 834: 211–213, 1999.

Werth JL, **Thayer SA**. Mitochondria buffer physiological calcium loads in cultured rat dorsal root ganglion neurons. *J Neurosci* 14: 348–356, 1994.

Whim MD, **Niemann H**, **Kaczmarek LK**. The secretion of classical and peptide cotransmitters from a single presynaptic neuron involves a synaptobrevin-like molecule. *J Neurosci* 17: 2338–2347, 1997.

White BH, **Kaczmarek LK**. Identification of a vesicular pool of calcium channels in the bag cell neurons of *Aplysia californica*. *J Neurosci* 17: 1582–1595, 1997.

de Wit H. Morphological docking of secretory vesicles. *Histochem Cell Biol* 134Springer Verlag: 103–113, 2010.

Woolum JC, **Strumwasser F**. Calcium changes in isolated peptidergic neurons during activation by a cAMP analog. *Brain Res* 444: 1–9, 1988.

Xia XM, **Fakler B**, **Rivard A**, **Wayman G**, **Johnson-Pais T**, **Keen JE**, **Ishii T**, **Hirschberg B**, **Bond CT**, **Lutsenko S**, **Maylie J**, **Adelman JP**. Mechanism of calcium gating in small-conductance calcium-activated potassium channels. *Nature* 395: 503–507, 1998.

Yang SN, **Berggren PO**. The role of voltage-gated calcium channels in pancreatic beta-cell physiology and pathophysiology. *Endocr Rev* 27: 621–676, 2006.

Yue DT, **Marban E**. Permeation in the dihydropyridine-sensitive calcium channel. Multi-ion occupancy but no anomalous mole-fraction effect between Ba^{2+} and Ca^{2+}. *J Gen Physiol* 95: 911–939, 1990.

Zamponi GW, **Bourinet E**, **Nelson D**, **Nargeot J**, **Snutch TP**. Crosstalk between G proteins and protein kinase C mediated by the calcium channel alpha1 subunit. *Nature* 385: 442–446, 1997.

Zazueta C, **Sosa-Torres ME**, **Correa F**, **Garza-Ortiz A**. Inhibitory properties of ruthenium amine complexes on mitochondrial calcium uptake. *J Bioenerg Biomembr* 31: 551–557, 1999.

Zenisek D, **Davila V**, **Wan L**, **Almers W**. Imaging calcium entry sites and ribbon structures in two presynaptic cells. *J Neurosci* 23: 2538–2548, 2003.

Zenisek D, **Matthews G**. The role of mitochondria in presynaptic calcium handling at a ribbon synapse. *Neuron* 25: 229–237, 2000.

Zhang Y, **Helm JS**, **Senatore A**, **Spafford JD**, **Kaczmarek LK**, **Jonas EA**. PKC-induced intracellular trafficking of Ca_V2 precedes its rapid recruitment to the plasma membrane. *J Neurosci* 28: 2601–2612, 2008.

Zühlke RD, **Pittt GS**, **Deisseroth K**, **Tsien RW**, **Reuter H**. Calmodulin supports both inactivation and facilitation of L-type calcium channels. *Nature* 399: 159–162, 1999.

Zühlke RD, **Reuter H**. Ca^{2+}-sensitive inactivation of L-type Ca^{2+} channels depends on multiple cytoplasmic amino acid sequences of the alpha1C subunit. *Proc Natl Acad Sci U S A* 95: 3287–3294, 1998.

Zurborg S, **Yurgionas B**, **Jira JA**, **Caspani O**, **Heppenstall PA**. Direct activation of the ion channel TRPA1 by Ca^{2+}. *Nat Neurosci* 10: 277–279, 2007.